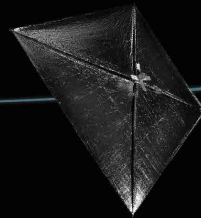


# Time-optimal solar sail transfers from Earth to pole-sitters at Mars and Venus

Master Thesis

Merel Vergaaij



Technische Universiteit Delft



# Time-optimal solar sail transfers from Earth to pole-sitters at Mars and Venus

by

Merel Vergaaij

Dissertation for the degree of

**Master of Science**

at The Astrodynamics and Space Missions Section,  
Delft University of Technology,  
to be defended publicly on Monday, March 5<sup>th</sup>, 2018.

Supervisor:	Dr. M. J. Heiligers	
Thesis committee:	Prof. dr. ir. P. N. A. M. Visser,	Committee chair
	Dr. M. J. Heiligers,	Supervisor
	Ir. P. P. Sundaramoorthy,	External examiner

*This thesis is confidential and cannot be made public until March 5<sup>th</sup>, 2019.*

An electronic version of this thesis will be available after March 5<sup>th</sup>, 2019 at  
<http://repository.tudelft.nl/>.



# Preface

This work marks the end of an era, the end of my time at the Delft University of Technology. This document is submitted in partial fulfillment of the requirements for the degree of Master of Science at the faculty of Aerospace Engineering. The work presented here provides time-optimal solar sail transfers from Earth to (quasi-)pole-sitters at Mars and Venus. The research is, to the best of my knowledge, original and I hope that it may be a meaningful contribution to the mission concept of planetary (quasi-)pole-sitters. Before we go ahead with this thesis work, I would like to take a moment to thank those who were important to me during the last few years.

First, I wish to thank the person who has had the most influence on my life in the past two years: Dr. Jeannette Heiligers. Without her advice, guidance, and encouragement, this work would not have been completed. I feel honored to have worked with her, not only during my thesis, but also during my internship at the Colorado Center for Astrodynamics Research. It was thanks to her enthusiasm and commitment that I got the opportunity to present our research at the International Astronautical Congress, which in turn led to the decision to write the main body of this thesis in a journal article format. During our weekly meetings, which I always looked forward to, she was always willing to answer all of my questions, not only regarding the thesis work, but also regarding conference etiquette, professional writing, a potential academic career, and country music. I am sure that all of my friends and family are wondering who this mysterious woman is I cannot stop talking about and they must be very happy that I am now taking the final step in graduating so they finally get to meet her.

I also wish to thank my friends and family for guiding me through my studies. I feel very lucky that there was always someone I could count on, talk to, blow off steam with, spend long days and nights in the library with, and bounce ideas off of. Thank you for keeping me motivated throughout my studies here in Delft and during the time I spent abroad.

Finally, I wish to thank all authors that have previously worked or are working on solar sailing. The concept of solar sailing never fails to impress me, and I sincerely hope that solar sails continue to cross boundaries and that, in the not-too-distant future, we will see the planetary (quasi-)pole-sitter mission come to fruition.

*Merel Vergaaij,  
Delft, March 2018*



# Abstract

This thesis work provides time-optimal solar sail transfers to pole-sitters and quasi-pole-sitters at Mars and Venus. A pole-sitter is a satellite positioned along the polar axis of a planet, providing a continuous hemispherical view of the polar region of the planet. This unique vantage point enables unprecedented continuous real-time medium-resolution observation of the polar region and provides opportunities for polar telecommunications. In order to maintain this vantage point, continuous thrust is required. Past work considered employing a hybrid combination of solar electric propulsion (SEP) and solar sailing to provide this thrust. Recent studies have shown the feasibility of the quasi-pole-sitter mission concept, which, contrary to the conventional pole-sitter mission, allows movement around the polar axis of the planet without compromising on the continuous hemispherical view of the polar region under a certain minimum elevation angle. If a solar sail with sufficient performance is employed, these quasi-pole-sitter orbits can be flown in a sail-only configuration, thus eliminating the need for propellant. The feasibility of the mission concept of planetary (quasi-)pole-sitters is contingent on the accessibility of these orbits. Therefore, this work focuses on transfers to selected pole-sitters and quasi-pole-sitters at Mars and Venus. The proposed transfers depart from a geostationary transfer orbit with perigee on the night-side of the Earth, where an initial impulsive burn brings the spacecraft to a parabolic escape trajectory. To completely eliminate the need for propellant for the remainder of the transfer, a solar sail is employed instead of high-thrust chemical propulsion or low-thrust electric propulsion (e.g., SEP).

Solar sails continuously generate thrust by reflecting solar photons off the large and highly reflective sail membrane. While solar sails are attractive due to their propellant-less nature, interplanetary solar sail transfers are known to span many years. To decrease mission operational costs, the objective of this work is to minimize the time of flight of the proposed transfers. This is done by solving an optimal control problem using an open-source direct pseudospectral method, PSOPT. In order to initialize this optimization, a (near-)feasible initial guess of the trajectory and the sail orientation over time is required. Historically, this initial guess is found using a grid search, which is one of the two techniques employed in this work to obtain the initial guess. The grid search used here is based on a technique derived from dynamical systems theory, where connections of stable and unstable invariant manifolds are sought for. In this work, solar sail dedicated sets are used, which are manifold-like structures where the dynamics of the system have been complemented with a solar sail induced acceleration. In addition, this work provides an investigation into the application of genetic algorithms to provide the initial guesses for the selected transfers, in order to assess and compare the performance of the two techniques. The two techniques cover both ends of the spectrum: the robust and proven technique from dynamical systems theory requires, to a certain degree, a-priori knowledge of the dynamical system used and the problem at hand, while the genetic algorithm requires no a-priori knowledge and is relatively new to the field of low-thrust trajectory optimization. Both techniques have to find the same parameters to construct the initial guesses: date and time at departure (directly linked to the initial state of the transfer), linkage of two interplanetary phases, and arrival (directly linked to the final state at the (quasi-)pole-sitter), and the orientation of the solar sail over time. The two techniques are compared in terms of feasibility of the initial guesses, computation time, and ease of implementation.

Using solar sail technology expected in a near- to mid-term time frame, transfers from the parabolic escape trajectory at Earth to the selected (quasi-)pole-sitters span 2.61 and 2.72 years to Mars and 1.07 and 1.19 years to Venus. Effects due to variations in performance of an ideal sail, inclusion of non-ideal sail properties, and Earth departure orbit are investigated. A nearly inversely proportional relationship is found between sail performance and transfer time, up to mid- to far-term sail technology. Introducing non-ideal sail properties comes with a modest penalty on the transfer time: a 10.8% increase in transfer time is observed to the hybrid pole-sitter at Mars. Finally, results show that for transfers spiraling outwards from the Earth (i.e., to Mars), perigee of the departure orbit should be on the day-side of the

Earth, whereas for transfers spiraling inwards from the Earth (i.e., to Venus) perigee should ideally be on the night-side of the Earth.

Furthermore, the two initial guess techniques both produce near-feasible and comparable initial guesses. However, in terms of feasibility of the initial guesses, computation time, and ease of implementation, the genetic algorithm outperforms the grid search and is therefore recommended for these particular types of transfers.

# Contents

<b>Nomenclature</b>	<b>ix</b>
<b>1 Introduction</b>	<b>1</b>
1.1 Research Questions . . . . .	2
1.2 Report Outline . . . . .	2
<b>2 Journal Article</b>	<b>5</b>
<b>3 Conclusions and Recommendations</b>	<b>37</b>
3.1 Conclusions . . . . .	37
3.2 Recommendations . . . . .	39
3.3 Implications . . . . .	40
<b>A Verification and Validation</b>	<b>41</b>
A.1 Dynamical Model . . . . .	41
A.1.1 Circular Restricted Three-Body Problem . . . . .	41
A.1.2 Solar Sail Models . . . . .	42
A.1.3 Fourth-Body Perturbation . . . . .	42
A.1.4 Reference Frame Transformations . . . . .	44
A.2 Initial Guess Techniques . . . . .	45
A.3 Time-Optimal Result . . . . .	45



# Nomenclature

## Abbreviations and Acronyms

AIAA	=	American Institute of Aeronautics and Astronautics
CR3BP	=	Circular Restricted Three-Body Problem
DST	=	Dynamical Systems Theory
GA	=	Genetic Algorithm
GTO	=	Geostationary Transfer Orbit
HM	=	Hybrid pole-sitter at Mars
HV	=	Hybrid pole-sitter at Venus
NLP	=	Non-Linear Programming
PSOPT	=	PSeudospectral OPTimizer
QM	=	Quasi-pole-sitter at Mars
QV	=	Quasi-pole-sitter at Venus
RNG	=	Random Number Generator
SE	=	Sun-Earth
SEP	=	Solar Electric Propulsion
SM	=	Sun-Mars
SOI	=	Sphere Of Influence
SV	=	Sun-Venus

## Latin Symbols

$a$	=	semi-major axis [km]
$\mathbf{a}$	=	acceleration vector in CR3BP [non-dim]
$A$	=	sail area [m <sup>2</sup> ]
$B$	=	non-Lambertian coefficient
$d$	=	distance [non-dim]
$e$	=	eccentricity
$f$	=	force [N]
$i$	=	inclination [deg]
$J$	=	cost function
$m$	=	mass [kg]
$\hat{\mathbf{n}}$	=	sail normal unit vector
$P$	=	radiation pressure [N/m <sup>2</sup> ]
$r$	=	position [km]
$\tilde{r}$	=	reflectivity constant
$\mathbf{r}$	=	position vector in CR3BP [non-dim]
$\hat{\mathbf{r}}, \hat{\boldsymbol{\theta}}, \hat{\boldsymbol{\phi}}$	=	unit vectors defining axes of sail fixed frame $B$
$s$	=	specular reflectivity fraction coefficient
$s_v$	=	scaling factor in fitness function
$t$	=	time [s], [non-dim]
$\mathbf{u}$	=	control vector [deg]
$v$	=	velocity [km/s]
$V$	=	gravitational potential CR3BP [non-dim]
$x, y, z$	=	position coordinates in CR3BP [non-dim]
$\mathbf{x}$	=	state vector in CR3BP [non-dim]
$\tilde{\mathbf{x}}$	=	state vector in heliocentric inertial frame [km, km/s]
$\hat{\mathbf{x}}, \hat{\mathbf{y}}, \hat{\mathbf{z}}$	=	unit vectors defining axes of CR3BP in frame $A$
$\mathbf{X}$	=	gene for genetic algorithm
$\hat{\mathbf{X}}, \hat{\mathbf{Y}}, \hat{\mathbf{Z}}$	=	unit vectors defining axes of heliocentric inertial frame $H$

$\hat{\mathbf{X}}_E, \hat{\mathbf{Y}}_E, \hat{\mathbf{Z}}_E$  = unit vectors defining axes of Cartesian Earth-centered inertial frame  $E$

### Greek Symbols

$\alpha$	=	cone angle [deg]
$\beta$	=	lightness number
$\delta$	=	clock angle [deg]
$\delta_{eq}$	=	obliquity of equator [deg]
$\Delta v$	=	change in velocity [km/s]
$\epsilon$	=	emissivity
$\theta$	=	pitch angle [deg]
$\vartheta$	=	true anomaly [deg]
$\lambda$	=	unit of length in CR3BP [km]
$\mu$	=	mass ratio
$\xi$	=	angular separation between $\hat{\mathbf{n}}$ and $\hat{\mathbf{m}}$ [deg]
$\tau$	=	unit of time in CR3BP [s]
$\phi$	=	angle between vernal equinox and planet [deg]
$\omega$	=	rotation rate [rad/s], [non-dim] or argument of periapsis [deg]
$\Omega$	=	right ascension of the ascending node [deg]
$\Omega_4$	=	fourth-body potential [non-dim]

### Subscripts

0	=	referring to initial time or state
1	=	larger primary
2	=	smaller primary
4	=	fourth body
arr	=	arrival
b	=	back side of sail
dep	=	departure
f	=	front side of sail or referring to final time or state
link	=	linkage
N	=	normal
s	=	sail
t	=	transfer
T	=	tangential
WS	=	winter solstice

### Superscripts

$(A), (B)$	=	expressed in reference frame $A$ or $B$
.	=	differentiation with respect to time
^	=	unit vector
~	=	expressed in dimensional quantities

# Introduction

A pole-sitter is a spacecraft that is positioned stationary along the polar axis of a planet. Such a vantage point provides a continuous hemispherical view of the polar regions of a planet, facilitating unparalleled applications in the field of telecommunications and monitoring of the polar regions, with unprecedented temporal resolution [1, 2]. However, the application of constant thrust is required in order to maintain this highly non-Keplerian orbit. Past studies [2–4] have considered using a hybrid combination of solar electric propulsion (SEP) and solar sailing to generate the thrust required for this type of mission, since the two propulsion methods compensate for each other's limitations. While the solar sail can only provide an acceleration away from the Sun, it lowers the amount of propellant needed for the SEP-system, which can provide the missing acceleration component towards the Sun [3, 5]. Recently, the mission concept of the hybrid pole-sitter has been extended with the notion of a quasi-pole-sitter [6], which relaxes the requirement of maintaining a position exactly on the polar axis and instead allows movement around the polar axis, without compromising on the continuous view of the Arctic region under a certain minimum elevation angle. If a solar sail with sufficient performance is employed, these quasi-pole-sitters can be flown in a solar sail-only configuration, which completely eliminates the need for propellant.

Solar sails [7] have attracted the interest of the scientific community as an advanced method of low-thrust propulsion due to its propellant-less nature: solar photons are reflected off the large and highly reflecting sail membrane, continuously generating thrust. Because of its working principle, solar sailing is capable of both potentially decreasing mission costs by eliminating or decreasing the need for propellant and therefore potentially decreasing launch mass [8, 9], and promoting the feasibility of previously unachievable or unrealistic missions [10, 11].

While the orbits for planetary (quasi-)pole-sitters have been studied in detail [6, 12], so far only transfers to pole-sitters at Earth have been investigated [13], leaving transfers to planetary pole-sitters at other planets unexplored. However, the feasibility of the mission concept of planetary (quasi-)pole-sitters hinges on the accessibility of these orbits at planets other than Earth. To this extent, this thesis work will focus on obtaining solar sail transfers from a parabolic escape trajectory at Earth to hybrid pole-sitters and sail-only quasi-pole-sitters at Mars and Venus. As solar sail interplanetary travel is known to span many years, in order to decrease mission operational costs, the duration of this transfer has to be minimized. This is done by seeking the solution to an optimal control problem using a particular implementation of a direct pseudospectral method, PSOPT [14], similar to previous work aimed at finding time-optimal solar sail heteroclinic connections between periodic orbits at the Moon and Mars [15] and the work done on transfers to Earth pole-sitters [13]. In order to initialize this optimization, an initial guess of the trajectory and the solar sail attitude over time is required. In this work, this initial guess is provided through two completely different methods in order to compare and validate the individual performances. On one end of the spectrum, a technique derived from dynamical systems theory is used, which is a robust and proven method, previously used for time-optimal Earth-Mars solar sail transfers [15, 16]. This technique employs a type of grid search to find a suitable near-feasible initial guess, which requires, to a certain degree, knowledge of the dynamical system used and the problem at hand. At the other end of the spectrum, a method is used that is relatively new in the field of low-thrust trajectory optimization, but is increasingly popular: a genetic algorithm. Genetic algorithms

have gained popularity and are a promising method to replace the more conventional grid search [17–19] for the first stage of trajectory optimization, because it requires no a-priori knowledge of the problem at hand. In order to further investigate the application of genetic algorithms for obtaining initial guess trajectories, this thesis work will provide a comparison of the two initial guess techniques in terms of feasibility of the initial guess solution, ease of implementation, and computation time.

The remainder of this chapter is focused on formulating research questions and subquestions associated with finding time-optimal solar sail transfers to hybrid and quasi-pole-sitters at Mars and Venus in Section 1.1, while an outline of this thesis report is given in Section 1.2.

## 1.1. Research Questions

The introduction to this thesis has shown that this thesis work is focused at finding time-optimal solar sail transfers from a parabolic escape trajectory to hybrid pole-sitters and quasi-pole-sitters at Mars and Venus, using two distinct initial guess techniques. To this extent, the following research questions and subquestions have been formulated:

1. **What is the minimum time of flight for a transfer from a departure orbit at Earth to a hybrid- or quasi-pole-sitter position at Mars or Venus when employing solar sailing as a means of propulsion?**
  - (a) **What is the effect of including optical imperfections in the solar sail model on the minimum-time transfer?**
  - (b) **What is the effect of improvements in solar sail technology in a mid- to far-term time frame on the minimum-time transfer?**
  - (c) **What is the effect of the orientation of the departure orbit on the minimum-time transfer?**
2. **How does the application of a genetic algorithm compare to the use of the more conventional grid search in obtaining an initial guess for a time-optimal solar sail transfer from Earth to Mars or Venus?**
  - (a) **How does a genetic algorithm compare to the grid search in terms of feasibility and optimality of the initial guess solution?**
  - (b) **How does a genetic algorithm compare to the grid search in terms of ease of implementation?**
  - (c) **How does a genetic algorithm compare to the grid search in terms of computation time?**

It is believed that, by answering these research questions, a substantial and valuable addition can be made to the mission concept of the (quasi-)pole-sitter and to the application of genetic algorithms for finding initial guess solutions for trajectory optimization problems.

## 1.2. Report Outline

To answer the research questions and subquestions posed in the previous section, the main part of this thesis report is written as a journal paper manuscript, ready to be submitted to the Journal of Guidance, Control and Dynamics, a peer-reviewed scientific journal published by the American Institute of Aeronautics and Astronautics (AIAA). The paper is titled:

”Time-Optimal Solar Sail Transfers to Pole-Sitters at Mars and Venus”

The paper manuscript can be found in Chapter 2, which is written according to the paper guidelines issued by the AIAA<sup>1</sup>. The paper starts with another abstract and introduction, after which the dynamical model will be explained. This is followed by the problem definition, optimal control problem, both initial guess techniques, and the obtained results. After a range of sensitivity analyses, the paper ends with the conclusion. This concludes the main part of this thesis report. In Chapter 3, the conclusion of

<sup>1</sup><https://www.aiaa.org/Tech-Presenter-Resources/>

---

the posed research (sub)questions will be given, alongside the recommendations for future work and the implications of this work. Finally, to support the numerical methods used throughout this work, verification and validation of the dynamical model, initial guess techniques, and time-optimal results can be found in Appendix A.



2

Journal Article

# Time-Optimal Solar Sail Transfers to Pole-Sitters at Mars and Venus

Merel Vergaaij\*

*Delft University of Technology, 2629 HS, Delft, The Netherlands*

Recent studies have shown the feasibility of (quasi-)pole-sitter orbits at Mars and Venus, which involves a satellite positioned along or near the polar axis of a planet in order to have a continuous, hemispherical view of the planet's polar regions. In order to further demonstrate the feasibility of this mission concept, this paper investigates time-optimal solar sail transfers to these (quasi-)pole-sitters. In particular, (quasi-)pole-sitters which are achievable when assuming solar sail technology expected in a near- to mid-term time-frame. To reduce mission operational cost, the objective of this research is to minimize the time required for the transfer, which requires the solution to an optimal control problem. Initial guess solutions for this optimal control problem are provided through two completely different techniques, in order to compare and validate the individual performances: first, a technique derived from dynamical systems theory (a type of grid search) and second, a genetic algorithm. Subsequent optimization using a direct pseudospectral algorithm results in time-optimal transfers to the considered Mars (quasi-)pole-sitters that span 2.61 and 2.72 years, and 1.07 and 1.19 years to the considered Venus (quasi-)pole-sitters. Effects due to variations in performance of the ideal sail, non-ideal sail properties, and Earth departure orbit are investigated. In addition, this paper demonstrates that a genetic algorithm is well suited to generate initial guesses for similar interplanetary transfers in the inner solar system. It provides initial guesses that outperform the more conventional grid search technique, in terms of feasibility of the initial guess transfers, as well as in computation time and ease of implementation.

## I. Introduction

WHILE the idea of solar sailing has been around for almost a century [1], it was not until recently that solar sailing truly took off with the first successful missions: JAXA's IKAROS mission (2010)[2], NASA's NanoSail-D2 mission (2010)[3], and The Planetary Society's LightSail-1 mission (2015)[4]. Contrary to conventional methods of propulsion, solar sailing transcends the dependence on the expulsion of mass by reflecting solar photons off a large and highly reflective membrane, generating continuous thrust. Because of this working principle, solar sails have in

---

\*Graduate Student, Department of Astrodynamics and Space Missions, Faculty of Aerospace Engineering, m.vergaaij@tudelft.nl.

principle unlimited  $\Delta v$  at their disposal, which is only constrained by the lifetime of the sail. High-energy and long-duration missions make optimal use of the capabilities of solar sailing, of which promising examples include highly non-Keplerian orbits [5–8], inner solar system rendezvous and sample return missions [9], advanced space weather warning mission concepts [10–12], and a solar polar orbiter [13]. Another example of a type of mission that greatly benefits from the high potential of solar sailing is a pole-sitter mission [14, 15].

A pole-sitter is a satellite that is positioned along the polar axis of a planet to generate a continuous, hemispherical view of the planet's polar regions. Such a view enables unique and unprecedented opportunities for polar observation and telecommunication. In order to preserve such a vantage point, a low-thrust propulsion system is required to counterbalance the gravitational attraction of the planet and the Sun [16]. Past studies have considered a hybrid combination of solar electric propulsion (SEP) and solar sailing [16–18]. These two systems complement each other: a solar sail can only provide an acceleration away from the Sun, but can do so without the need for propellant, while the SEP-system provides the missing acceleration component towards the Sun [17, 19].

A derivative of the pole-sitter concept relaxes the requirement that the spacecraft has to be positioned exactly along the polar axis of the planet and instead allows a slight movement around the polar axis, without compromising on the continuous view of the entire polar region at a certain minimum elevation angle [15]. If a sail with sufficient performance is employed, this quasi-pole-sitter mission can even be achieved without the need for an SEP-system.

Whereas previous research on pole-sitters at planets other than Earth has focused on optimizing the pole-sitter orbit for minimum propellant mass (hybrid propulsion pole-sitter) [20] or minimum planet-sail distance (sail-only quasi-pole-sitter) [15], this research is aimed at optimizing the transfer from Earth to these optimized planetary (quasi-)pole-sitter orbits. The accessibility of pole-sitters at Earth has been analyzed before for both high-thrust and low-thrust departure trajectories from low Earth orbit [21], but the design of solar sail transfers to pole-sitters at planets other than Earth remains unexplored. To this extent, this paper will investigate time-optimal solar sail transfers to (quasi-)pole-sitter orbits at Mars and Venus, since the feasibility of the (quasi-)pole-sitter mission concept hinges on the accessibility of these orbits.

These time-optimal transfers are sought for by solving an optimal control problem. In order to solve this optimal control problem, a (near-)feasible initial guess has to be provided, which is very important for the optimizer to converge. In this work, initial guesses are found using two separate techniques for validation and comparison purposes. First, using a technique similar to the work done in References [22, 23], relying on a technique derived from dynamical systems theory, and second, using a genetic algorithm. Solving the optimal control problem is achieved by using an open source direct pseudospectral algorithm, PSOPT [24].

The structure of this paper is as follows. First, the components of the dynamical model that are used in this work are described in detail, including the circular restricted three-body problem, the solar sail model, the modeling of fourth-body perturbations, and the implementation of ephemerides. Next, the problem to be solved is defined, including

the departure orbit and the definition of the pole-sitter orbit. Subsequently, the associated optimal control problem is defined, and a description of the optimal control solver is given. This is followed by an explanation of the two methods used to obtain the initial guesses, a presentation of the obtained initial guesses, and a discussion on the two initial guess techniques and the obtained initial guesses. Finally, the time-optimal results are presented and a range of sensitivity analyses is described in detail. The paper ends with the conclusions.

## II. Dynamical Models

This section describes the dynamical framework that is used in this work. Section II.A defines the circular restricted three-body problem (CR3BP), which has also been used to construct and optimize the (quasi-)pole-sitter orbits [15, 17]. In Section II.B the solar sail models for a perfectly reflecting (i.e., ideal) sail and an optical (i.e., non-ideal) sail are described, followed by the implementation of fourth-body perturbations and the ephemerides in Section II.C and II.D, respectively.

### A. Circular Restricted Three-Body Problem

Following previous work [15, 21], the dynamical system employed in this research is the CR3BP, which describes the motion of an infinitesimally small mass,  $m$ , under the influence of two much larger masses,  $m_1$  (here the Sun) and  $m_2$  (here the planet), where  $m_1$  is the larger mass of the two primaries. The two primaries move in circular orbits around the barycenter of the system and the gravitational influence of the small mass on the primaries is neglected [25].

The reference frame employed,  $A(\hat{x}, \hat{y}, \hat{z})$ , is a synodic frame, rotating around the barycenter of the two primaries, see Fig. 1. The  $\hat{x}$ -axis connects the two primaries and points towards  $m_2$ , the  $\hat{z}$ -axis is directed perpendicular to the orbital plane of the primaries, and the  $\hat{y}$ -axis completes the right-handed Cartesian reference frame. The frame rotates around the  $\hat{z}$ -axis at a constant angular velocity,  $\omega = \omega\hat{z}$ . The distance from the first primary to  $m$  is denoted by  $r_1$  and from the second primary to  $m$  by  $r_2$ , as shown in Fig. 1.

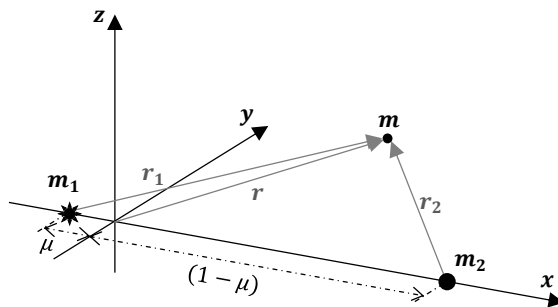


Fig. 1 Schematic of the Sun-planet CR3BP in reference frame A.

The dynamics of the CR3BP are non-dimensionalized using the sum of the masses of the two primaries as the unit of mass, the distance between the primaries as the unit of length,  $\lambda$ , and  $1/\omega$  as the unit of time,  $\tau$ . Using the mass ratio  $\mu = m_2/(m_1 + m_2)$ , the dimensionless masses of the primaries become  $m_1 = (1 - \mu)$  and  $m_2 = \mu$ , and their location along the  $\hat{\mathbf{x}}$ -axis becomes  $-\mu$  and  $(1 - \mu)$ , respectively. Because  $\tau$  is used to non-dimensionalize the time,  $\omega = 1$ , which implies that one orbital period of the primaries around the barycenter is equal to  $2\pi$ . Values for  $\mu$ ,  $\lambda$ , and  $\tau$  can be found in Table 1 for the Sun-Earth (SE), Sun-Mars (SM), and Sun-Venus (SV) CR3BPs.

**Table 1 CR3BP parameters.**

	SE-CR3BP	SM-CR3BP	SV-CR3BP
$\mu$ [-]	$3.003460 \cdot 10^{-6}$	$3.226835 \cdot 10^{-7}$	$2.447819 \cdot 10^{-6}$
$\lambda$ [km]	$1.4960 \cdot 10^8$	$2.2794 \cdot 10^8$	$1.0821 \cdot 10^8$
$\tau$ [s]	$5.016278 \cdot 10^6$	$9.446103 \cdot 10^6$	$3.089778 \cdot 10^6$

The motion of the infinitesimally small mass in the CR3BP is described by the following set of equations of motion [26]:

$$\ddot{\mathbf{r}} + 2\boldsymbol{\omega} \times \dot{\mathbf{r}} + \boldsymbol{\omega} \times (\boldsymbol{\omega} \times \mathbf{r}) + \nabla V = \mathbf{a}, \quad (1)$$

where the left-hand side represents the ballistic CR3BP, for which the gravitational potential,  $V$ , is calculated as:

$$V = \frac{1 - \mu}{r_1} - \frac{\mu}{r_2}. \quad (2)$$

The right-hand side of Eq. (1),  $\mathbf{a}$ , is the acceleration due to external forces. In this work,  $\mathbf{a}$  includes the acceleration induced by the solar sail and fourth-body gravitational perturbations.

## B. Solar Sail Model

Solar sails exploit the solar radiation pressure induced by solar photons reflecting off the sail to produce a force, and thus an acceleration. In this work, two different sail models are adopted: an ideal sail and an optical sail [1]. While an ideal sail assumes perfect, specular reflection of the incoming solar photons, the optical sail model takes diffuse reflection, absorption, and emission by re-radiation into account. The dynamical model associated with these solar sail models are discussed separately in the next two subsections.

### 1. Ideal sail

As mentioned, an ideal sail assumes pure specular reflection of the incident radiation. The resulting acceleration then acts normal to the sail surface, along  $\hat{\mathbf{n}}$ , defined in Fig. 2 [1]. To uniquely define the direction of the sail normal in space, reference frame  $B(\hat{\mathbf{r}}_1, \hat{\boldsymbol{\theta}}, \hat{\boldsymbol{\phi}})$  is introduced, defined by a set of three orthogonal vectors  $\{\hat{\mathbf{r}}_1, \hat{\mathbf{z}} \times \hat{\mathbf{r}}_1, \hat{\mathbf{r}}_1 \times (\hat{\mathbf{z}} \times \hat{\mathbf{r}}_1)\}$ , with its origin at the position of the sail, see Fig. 2 [27]. The sail normal vector,  $\hat{\mathbf{n}}$ , in frame  $B$  can then be expressed

through the cone angle,  $\alpha$ , and the clock angle,  $\delta$ :

$$\hat{\mathbf{n}}^{(B)} = \begin{bmatrix} \cos(\alpha) \\ \sin(\alpha) \sin(\delta) \\ \sin(\alpha) \cos(\delta) \end{bmatrix}, \quad (3)$$

which can be transformed to frame  $A$  through:

$$\hat{\mathbf{n}}^{(A)} = \begin{bmatrix} \hat{\mathbf{r}}_1 & \hat{\boldsymbol{\theta}} & \hat{\boldsymbol{\phi}} \end{bmatrix} \hat{\mathbf{n}}^{(B)}. \quad (4)$$

Using  $\hat{\mathbf{n}}$  (superscript  $(A)$  is omitted from here on), the solar sail induced acceleration in frame  $A$  of the CR3BP can be calculated:

$$\mathbf{a}_s = \beta \frac{1-\mu}{r_1^2} (\hat{\mathbf{r}}_1 \cdot \hat{\mathbf{n}})^2 \hat{\mathbf{n}}, \quad (5)$$

where it can be seen that the acceleration is proportional to the non-dimensional solar gravitational acceleration,  $\frac{1-\mu}{r_1^2}$ , and is scaled by  $\beta$ , the lightness number. The lightness number is then defined as the ratio of the acceleration due to solar radiation pressure and the solar gravitational acceleration [1]. In a near- to mid-term time-frame, the value for the lightness number is expected to be 0.05 [28], while in a mid- to far-term time-frame, values for  $\beta$  are expected to go to as high as 0.1 [29].

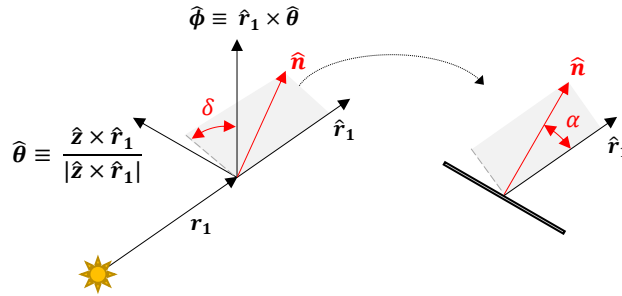


**Fig. 2 Definition of solar sail normal vector,  $\hat{\mathbf{n}}$ , in reference frame B [23].**

## 2. Optical Sail

In the case of an optical sail, not just specular reflection, but also diffuse reflection, absorption, and re-emission by re-radiation of the incident photons are taken into account. These additional incorporated effects cause a component of the acceleration tangential to the sail, resulting in an acceleration deviating from the sail normal, which instead acts along  $\hat{\mathbf{m}}$ , see Fig. 3 [1]. This effect increases for increasing cone angles. In order to calculate the optical sail induced acceleration, the pitch angle  $\theta$  is introduced, see again Fig. 3. Where for the ideal sail the pitch angle is equal to the

cone angle,  $\alpha$ , this is not the case for an optical sail. Instead, the pitch angle for an optical sail is calculated using the magnitude of the forces normal and tangential to the sail,  $f_N$  and  $f_T$ , respectively. These are determined using [1]:

$$f_N = PA \left[ (1 + \tilde{r}s) \cos^2 \alpha + B_f(1 - s)\tilde{r} \cos \alpha + (1 - \tilde{r}) \frac{\epsilon_f B_f - \epsilon_b B_b}{\epsilon_f + \epsilon_b} \cos \alpha \right], \quad (6a)$$

$$f_T = PA(1 - \tilde{r}s) \cos \alpha \sin \alpha, \quad (6b)$$

where  $P$  is the radiation pressure,  $A$  the sail area,  $\tilde{r}$  the total reflectivity constant,  $s$  the specular reflectivity fraction coefficient,  $\epsilon$  the emissivity, and  $B$  the non-Lambertian coefficient for the front (subscript  $f$ ) and back side (subscript  $b$ ) of the sail. Values for each of the optical sail coefficients can be found in Table 2. The angular separation between  $\hat{\mathbf{m}}$  and  $\hat{\mathbf{n}}$ ,  $\xi$ , and subsequently the pitch angle, can be calculated as:

$$\xi = \tan^{-1} \left( \frac{f_T}{f_N} \right), \quad (7a)$$

$$\theta = \alpha - \xi. \quad (7b)$$

Substituting  $\theta$  for  $\alpha$  in Eq. (3) yields the direction of  $\hat{\mathbf{m}}$ , as shown in Fig. 3. This only leaves the dimensionless solar sail acceleration magnitude to be computed, resulting in the following optical sail acceleration:

$$\mathbf{a}_s = \frac{\beta}{2} \frac{1 - \mu}{r_1^2} \sqrt{\left[ \frac{f_N}{PA} \right]^2 + \left[ \frac{f_T}{PA} \right]^2} \hat{\mathbf{m}}. \quad (8)$$

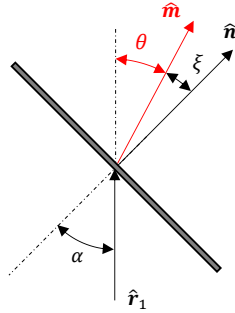


**Fig. 3** Definition of direction of solar sail induced acceleration for an optical sail,  $\hat{\mathbf{m}}$ .

**Table 2** Optical sail coefficients [30].

Coefficient	$\tilde{r}$	$s$	$B_f$	$B_b$	$\epsilon_f$	$\epsilon_b$
Value	0.91	0.94	0.79	0.67	0.025	0.27

### C. Fourth-Body Perturbations

As will become clear in Section IV, the Earth-Venus and Earth-Mars transfers are designed by patching different CR3BPs. For example, for the Earth-Mars transfers, the transfer starts in the SE-CR3BP and is switched to the SM-CR3BP later on in the transfer. This introduces a discontinuity in the dynamics. Therefore, to ensure that the dynamics are more consistent along the trajectory, fourth-body perturbations are included in the right-hand side of Eq. (1). The perturbing acceleration from a fourth body is calculated as [31]:

$$\mathbf{a}_4 = \frac{\partial \Omega_4}{\partial \mathbf{r}_4} \quad (9)$$

with

$$\Omega_4 = \mu_4 \left( \frac{1}{|\mathbf{r}_{s,4}|} - \frac{\mathbf{r} \cdot \mathbf{r}_4}{|\mathbf{r}_4|^3} \right) \quad (10)$$

where  $\mathbf{r}_4$  is the position vector from the barycenter of the CR3BP to the fourth body, defined in Section II.D, and  $\mathbf{r}_{s,4}$  the position vector from the sail to the fourth body. Subsequently,  $\mathbf{r}_{s,4} = \mathbf{r}_4 - \mathbf{r}$ . Finally,  $\mu_4$  is the dimensionless gravitational parameter of the fourth body, with values given in Table 3. Not all planets are included as fourth bodies in each system, only the bodies listed in Table 3.

**Table 3 Fourth-body perturbation parameters.**

Transfer	Patched CR3BPs	Perturbing body	$\mu_4$ [-]
Earth-Venus	SE-CR3BP	Venus	$2.447817 \cdot 10^{-6}$
	SV-CR3BP	Earth	$3.003462 \cdot 10^{-6}$
Earth-Mars	SE-CR3BP	Mars	$3.226827 \cdot 10^{-7}$
	SM-CR3BP	Earth	$3.003468 \cdot 10^{-6}$

### D. Ephemerides

In order to compute the fourth-body perturbation, the position of the fourth body in the target CR3BP has to be known at time  $t$ . For this, the fourth bodies are assumed to move in circular orbits in the ecliptic plane about the barycenter of their respective CR3BPs. To calculate the state vector of the fourth body in the CR3BP,  $\mathbf{r}_4$ , first, the state vector of the fourth body is given in its own CR3BP by:

$$\mathbf{x} = \begin{bmatrix} (1 - \mu) & 0 & 0 & 0 & 0 & 0 \end{bmatrix}^T, \quad (11)$$

which is transformed using the sequence described in Appendix A to an intermediate heliocentric inertial reference frame  $H(\hat{\mathbf{X}}, \hat{\mathbf{Y}}, \hat{\mathbf{Z}})$ , where the  $\hat{\mathbf{X}}$ -axis points towards the vernal equinox, the  $\hat{\mathbf{Z}}$ -axis is directed perpendicular to the ecliptic plane, and the  $\hat{\mathbf{Y}}$ -axis completes the right-handed reference frame. Finally,  $\mathbf{r}_4$  is calculated by transforming the state in the heliocentric inertial reference frame to the target CR3BP, according to the transformation described in Appendix B.

### III. Problem Definition

This paper will investigate and optimize transfers to (quasi-)pole-sitters. Section III.A will therefore describe and present the (quasi-)pole-sitter orbits that will be used in this work. It is furthermore assumed that the transfer starts from an Ariane V geostationary transfer orbit (GTO), hence Section III.B will elaborate on this orbit.

In addition, the following assumptions are made:

- 1) The lightness number,  $\beta$ , discussed in Section II.B, is assumed to be 0.05, which is representative of solar sail technology in a near- to mid-term time frame.
- 2) An ideal sail model is assumed.
- 3) The departure condition at Earth is constrained to perigee of a midnight-GTO, which will be explained in more detail in Section III.B, similar to the work in Reference [10].

The impact of these assumptions will be discussed later, in Section VII, where, for example, the effect of employing an optical sail model rather than an ideal sail model is investigated.

#### A. (Quasi-)Pole-Sitter Orbit

As stated in the introduction, a pole-sitter is a spacecraft that is positioned along the polar axis of a planet. In the synodic frame of the CR3BP, the polar axis spans a full conical surface every year due to the obliquity of the planet's equator with respect to the ecliptic,  $\delta_{eq}$ , see Fig. 4.

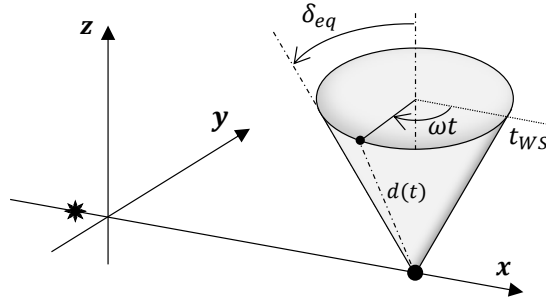


Fig. 4 Schematic for the pole-sitter orbit in the Sun-planet CR3BP.

The cone half angle is the tilt of the polar axis relative to the ecliptic (for Mars:  $\delta_{eq} = 25.19^\circ$ , and for Venus:  $\delta_{eq} = -177.36^\circ$ ). With no loss of generality, the state at winter solstice (at time  $t = t_{WS}$ ) is taken as the initial state of the pole-sitter. Then, the instantaneous position of the pole-sitter spacecraft at the non-dimensional time  $t$  is given by [17]:

$$\mathbf{r}(t) = \begin{bmatrix} d(t) \sin \delta_{eq} \cos [\omega(t - t_{WS})] + (1 - \mu) \\ -d(t) \sin \delta_{eq} \sin [\omega(t - t_{WS})] \\ d(t) \cos \delta_{eq} \end{bmatrix} \quad (12)$$

where  $d(t)$  is the distance from the center of the planet, which is a continuous function of time. To follow this trajectory, the pole-sitter utilizes a hybrid combination of a solar sail and an SEP-system. When allowing a slight deviation from the polar axis, without compromising on the visibility of the planet's entire Arctic region under a certain minimum elevation angle, a quasi-pole-sitter results [15]. For a good enough performance of the sail, this trajectory can be flown using only a solar sail, i.e., without the need for an SEP-thruster and therefore without any propellant consumption. Details on the constraints for the quasi-pole-sitter can be found in Reference [15]. The optimal (quasi-)pole-sitters from Reference [15] that are used in this work as final conditions of the transfer are the following, see Fig. 5:

**HM** Hybrid variable altitude pole-sitter at Mars,  $\beta = 0.05$ , optimized for propellant consumption of the SEP-system.

**HV** Hybrid variable altitude pole-sitter at Venus,  $\beta = 0.05$ , optimized for propellant consumption of the SEP-system.

**QM** Solar sail-only quasi-pole-sitter at Mars,  $30^\circ$  minimum elevation angle,  $\beta = 0.05$ , optimized for minimum  $d(t)$ .

**QV** Solar sail-only quasi-pole-sitter at Venus,  $30^\circ$  minimum elevation angle,  $\beta = 0.06$ , optimized for minimum  $d(t)$ .

Note that for case QV, the value for  $\beta$  is not congruent with the assumptions, which is due to the fact that for a performance of  $\beta = 0.05$  it is not possible to maintain a solar sail-only quasi-pole-sitter at Venus.

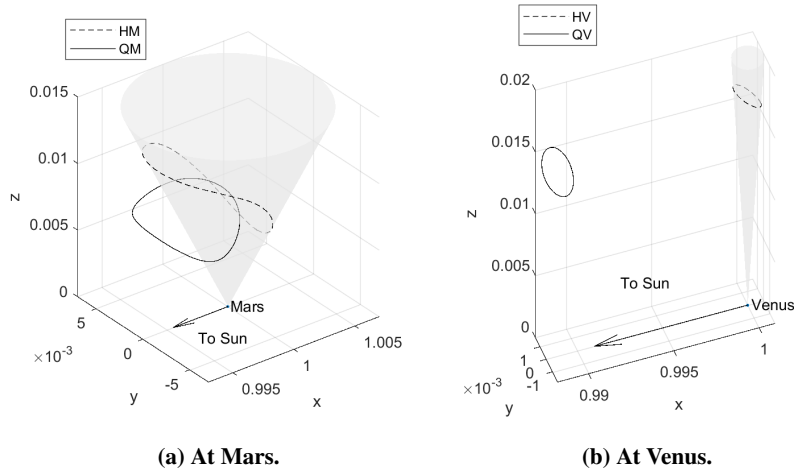


**Fig. 5 (Quasi-)pole-sitters in the SM- and SV-CR3BPs from Reference [15] that are used as target orbits in this work.**

## B. Earth Departure Orbit

In this work the spacecraft is assumed to be launched towards Mars or Venus from a midnight-GTO by an Ariane V launch vehicle, by applying a  $\Delta v$  at perigee of the GTO. For a midnight-GTO, the perigee of the GTO is located at the night side of the Earth [10]. The departure phase, up to the sphere of influence (SOI) of the Earth, is modeled as a ballistic arc in a two-body Cartesian Earth-centered inertial reference frame  $E(\hat{\mathbf{X}}_E, \hat{\mathbf{Y}}_E, \hat{\mathbf{Z}}_E)$ , with the  $\hat{\mathbf{X}}_E$ -axis pointing towards the vernal equinox, the  $\hat{\mathbf{Z}}_E$ -axis along the polar axis, and the  $\hat{\mathbf{Y}}_E$ -axis completing the right-handed reference frame.

The state at the SOI of the Earth in the SE-CR3BP can then be determined using the following steps:

- 1) First, the classical orbital elements at perigee of the GTO are calculated from the Ariane V manual [32]:  $a = 24467.508$  km,  $e = 0.7293959$ ,  $i = 6^\circ$ ,  $\omega = 178^\circ$ ,  $\vartheta = 0^\circ$ , and  $\Omega$  is taken arbitrarily at  $0^\circ$ . These orbital elements are defined in frame  $E$  and transformed to Cartesian coordinates.
- 2) Next, the state is rotated around the  $\tilde{Z}_E$ -axis such that perigee is exactly on the Sun-Earth line, behind the Earth, to ensure a midnight-GTO. Note that for a given departure date and time, this initial state of the transfer, at perigee of the midnight-GTO, is fixed.
- 3) Subsequently, an impulse of  $\Delta v = 0.7692916$  km/s is applied along the velocity vector at perigee of the midnight-GTO, which brings the spacecraft to a parabolic escape trajectory. This Cartesian state at perigee is then transformed back to classical orbital elements.
- 4) Finally, the true anomaly of the *parabolic* escape trajectory at the SOI of the Earth,  $\vartheta_{SOI}$ , can be found from (derived from [33]):

$$\vartheta_{SOI} = \cos^{-1} \left( \frac{2r_{perigee}}{r_{SOI}} - 1 \right), \quad (13)$$

where  $r_{perigee}$  is the radius at perigee and  $r_{SOI}$  the radius at the SOI. The state in orbital elements, including  $\vartheta_{SOI}$ , is then transformed back to Cartesian coordinates and from the frame  $E$  to the SE-CR3BP frame, according to the transformation sequence described in Appendix C, at which point the dynamics are complemented with the solar sail induced acceleration.

## IV. Optimal Control

For the problem defined in the previous section, the objective is to minimize the overall time spent in the transfer in order to reduce mission operational costs. This requires the solution to an optimal control problem, which will be defined in Section A, followed by a description of the optimal control solver used in this work, in Section B.

### A. Optimal Control Problem

In order to minimize the time spent in the transfer, the objective function is given by:

$$J = t_f - t_0, \quad (14)$$

where  $t_f$  and  $t_0$  are the final time at the (quasi-)pole-sitter and the initial time at perigee of the midnight-GTO, respectively.

Along the trajectory, the state,  $\mathbf{x}(t)$ , and controls,  $\mathbf{u}(t)$ , of the spacecraft are defined as:

$$\mathbf{x}(t) = \begin{bmatrix} x & y & z & \dot{x} & \dot{y} & \dot{z} \end{bmatrix}^T \quad (15a)$$

$$\mathbf{u}(t) = \begin{bmatrix} \alpha & \delta \end{bmatrix}^T \quad (15b)$$

where  $\mathbf{x}(t)$  is defined in the respective CR3BP, and bounds on the controls are defined as  $0^\circ \leq \alpha \leq 90^\circ$  and  $-180^\circ \leq \delta \leq 180^\circ$ .

The separate segments of the transfer are most accurately described in two different CR3BPs, since the departure trajectory after leaving the SOI of the Earth is modeled in the SE-CR3BP and the (quasi-)pole-sitters in the SM- and SV-CR3BPs. Therefore, the dynamics are split into two separate phases. For the Mars (quasi-)pole-sitter, the first phase is defined in the SE-CR3BP, whereas the second phase is defined in the SM-CR3BP. For the Venus (quasi-)pole-sitter, the phases are defined in the SE- and SV-CR3BPs. In order to guarantee a continuous transfer, smooth linkage of the two phases is required for the states, controls, and time. The states are linked after they are transformed to the heliocentric inertial frame  $H(\hat{\mathbf{X}}, \hat{\mathbf{Y}}, \hat{\mathbf{Z}})$ , where the state is denoted by  $\tilde{\mathbf{x}}$ , using the transformation described in Appendix A. The controls can be linked without a transformation, as the cone and clock angles are defined with respect to the Sun-sail line. So, if the states and controls are properly linked, the attitude of the sail is continuous across the linkage. Linkage of time is done in dimensional time (in seconds after 1-1-2000 noon),  $\tilde{t}$ , which results in a total of 9 linkage constraints:

$$\tilde{\mathbf{x}}_{f_1} = \tilde{\mathbf{x}}_{0_2}, \quad (16a) \quad \mathbf{u}_{f_1} = \mathbf{u}_{0_2}, \quad (16b) \quad \tilde{t}_{f_1} = \tilde{t}_{0_2}, \quad (16c)$$

where subscript  $f_1$  refers to the final conditions of the first phase and subscript  $0_2$  to the initial conditions of the second phase.

In addition to the constraints in Eq (16), boundary conditions are enforced to ensure that the initial state coincides with perigee of the midnight-GTO and the final state with the (quasi-)pole-sitter orbit. As was mentioned in Sections III.A and III.B, the departure and arrival time correspond directly to the required states at these boundaries. Furthermore, since the controls and time are free at the boundaries, the total number of boundary constraints for this problem is 12.

## B. Optimal control solver

The optimal control solver employed in this work is the open source software package PSOPT, a pseudospectral method that uses direct collocation methods [24]. The optimal control problem is solved by approximating the time-dependent variables using Legendre polynomials, at and between the collocation points, which are spaced according to Legendre-Gauss-Lobatto points. This way, the infinite dimensional optimal control problem is discretized into a finite number of collocation points, and the resulting finite dimensional non-linear programming (NLP) problem can be solved using IPOPT, an open source interior point optimizer for large scale NLP problems [34].

The problem defined in Section IV.A exhibits the following characteristics: a multiphase problem, with bounds on controls, state, and time variables, an end-point cost function, phase linkage constraints, boundary constraints, and a free initial and final time. PSOPT is capable of dealing with all of these characteristics [24].

## V. Initial Guess Techniques

As PSOPT requires an initial guess for initialization, the optimization process is divided into two steps. The first step aims at finding an initial guess, whereas the second step conducts a local optimization of this initial guess. The first step is performed using two different techniques, which will later be assessed on the quality of the initial guesses, ease of implementation, and computation time. This section will explain these two techniques, which are a technique derived from dynamical systems theory, as used in [23], and an approach based on a genetic algorithm.

To construct an initial guess for the transfer under consideration, several parameters have to be found: departure time ( $t_{dep}$ ), arrival time ( $t_{arr}$ ), time at linkage of the two CR3BPs ( $t_{link}$ ), and the orientation of the sail ( $\alpha$  and  $\delta$ ) over time. Note that, in the following, small discontinuities in position and velocity at the linkage of the two CR3BPs are allowed for the initial guess, as these will be overcome during the optimization in the second step.

To limit the search space, the following reasonable bounds are set on some of these parameters:

- Since fourth-body perturbations are not included in this part of the optimization process, linkage is only allowed to occur between 25% and 75% of the total transfer time.
- A minimum and maximum transfer time,  $t_{min}$  and  $t_{max}$ , are set to avoid unfeasible or undesirable transfers, without restricting the techniques from finding a (near-)feasible initial guess. For the Earth-Mars and Earth-Venus transfers,  $t_{min}$  is set to 1.5 years and 0.8 years, while  $t_{max}$  is set to 5 years and 3.5 years, respectively.

### A. Technique from Dynamical Systems Theory

The design technique from dynamical systems theory, hereafter referred to as DST-technique, is based on the use of invariant manifolds for the design of interplanetary transfers, where connections between stable and unstable invariant manifolds are sought for. Here, *solar sail dedicated sets* are used, which are types of manifolds-like structures where the dynamics of the system has been complemented with the solar sail induced acceleration. Invariant manifolds are created by propagating different initial conditions along the stable and unstable eigenvectors of periodic orbits, thereby creating a set of trajectories that forms a topological tube. In this work, similar topological tubes are created by forward and backward integration of different initial conditions along the (quasi-)pole-sitter or midnight-GTO. These initial conditions correspond to a range of departure and arrival times. Note that, as was stated in Section III, the departure time corresponds directly to a state at perigee of the midnight-GTO, while the arrival time corresponds directly to a state at the (quasi-)pole-sitter. For more details on the technique, the reader is referred to [22] and [23].

The shape of the topological tubes can be altered by considering different sail orientations, with practically unlimited possibilities. To limit the search space, the DST-technique assumes a constant orientation of the sail along the manifold and a fixed clock angle, since varying both the cone and the clock angle would add another dimension to the search space, which would have a profound negative impact on the computation time. To maximize the acceleration in the ecliptic plane, the clock angle is kept constant at  $90^\circ$  for the Earth-Mars transfers and at  $-90^\circ$  for the Earth-Venus

transfers [1]. For each constant sail orientation, the following steps are taken:

- 1) Set bounds for  $t_{dep}$ , spanning one synodic Earth-planet period starting from 1-7-2020 for the Earth-Mars transfers and 1-7-2021 for the Earth-Venus transfers. Based on these values for  $t_{dep}$  and the allowable transfer times,  $t_{min}$  and  $t_{max}$ , set bounds for  $t_{arr}$ . Next, create a grid for  $t_{dep}$  and  $t_{arr}$  of  $n$  equidistant values between these bounds.
- 2) Forward propagate the departure solar sail dedicated set, from all  $n$  values for  $t_{dep}$  to  $(t_{dep} + t_{max})$  in the SE-CR3BP.
- 3) Backward propagate the arrival solar sail dedicated set, from all  $n$  values for  $t_{arr}$  to  $(t_{arr} - t_{max})$  in the SM- or SV-CR3BP, depending on the (quasi-)pole-sitter considered.
- 4) For all  $n \times n$  combinations of the departure and arrival trajectories, determine  $n_{link}$  equally spaced values for  $t_{link}$ , between 25% and 75% of the total transfer time. Then, transform the states of the departure and arrival trajectories at all  $n_{link}$  values of  $t_{link}$  to the heliocentric inertial reference frame.
- 5) For all  $n \times n$  combinations of the departure and arrival trajectories, calculate the error in position ( $\Delta r$ ) and velocity ( $\Delta v$ ) at linkage for all  $n_{link}$  values of  $t_{link}$ . The errors of the transfer with the smallest position error are then stored for all  $n \times n$  combinations.

For a given sail orientation, the results of the procedure above can be visualized as in Fig. 6 for the HM case for a constant sail orientation of  $\alpha = 54^\circ$  and  $\delta = 90^\circ$ . From these figures and the corresponding data, it is possible to narrow down the search space, ultimately resulting in a near-feasible transfer from the midnight-GTO to the (quasi-)pole-sitter. The parameters and minor discontinuities at linkage for the initial guess found using this DST-technique are displayed in Table 4.

**Table 4 Initial guesses produced using the DST-technique, along with the associated discontinuities at linkage and transfer times.**

	HM	QM	HV	QV
$t_{dep}$	6-11-2021	14-10-2021	26-1-2021	7-6-2021
$t_{arr}$	26-9-2024	17-8-2024	16-10-2022	22-7-2022
$t_{link}$	24-7-2023	30-4-2023	13-8-2021	6-2-2022
$\alpha$ [deg]	42	45	58	51
$\delta$ [deg]	90	90	-90	-90
$\Delta r$ [km]	$8.9803 \cdot 10^5$	$1.3200 \cdot 10^6$	$1.0967 \cdot 10^6$	$1.1007 \cdot 10^6$
$\Delta v$ [km/s]	0.31724	0.27677	0.62862	0.75898
$t_t$ [years]	2.8863	2.8436	1.7191	1.1234

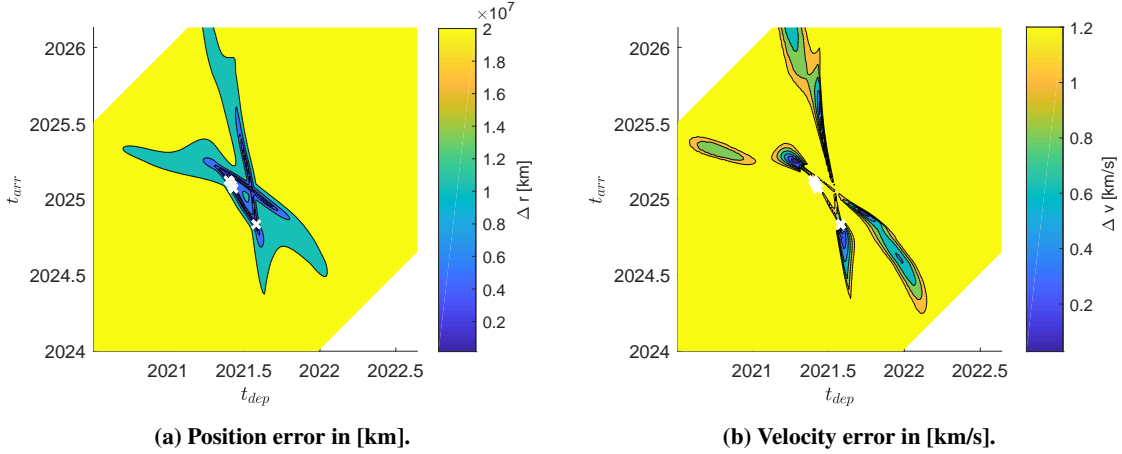


**Fig. 6** Example DST-technique result for HM pole-sitter transfer with  $\alpha = 54^\circ$ ,  $\delta = 90^\circ$ . White crosses mark the five best linkage conditions in terms of position.

## B. Genetic Algorithm

While the DST-technique is a robust and proven method [22, 23], it demands a substantial and detailed understanding of the dynamics, the problem at hand, and how to narrow down the search space, in order to produce a (near-)feasible initial guess. Directly opposite to this is a genetic algorithm, for which practically no a priori knowledge is required, and which is simple to implement [35]. Because optimal control solvers are known to be sensitive to the initial guess provided [35], using these two completely different methods allows for verification of the initial guess and the resulting time-optimal transfer.

The application of genetic optimization methods for low-thrust trajectory optimization has become increasingly popular, especially in the early stages of the mission design. As calculus-based approaches are generally not effective during this early stage, an exhaustive grid search, like the one explained in the previous section, has been the de facto standard to sort through the large set of possible solutions. Genetic algorithms are a promising method to replace this grid search [35–38]. Though rarely used by itself for low-thrust trajectory optimization, they are increasingly being used in combination with other optimization techniques [39–41], which is the approach taken here as well, as it is merely used as a technique to find an initial guess.

Genetic algorithms determine an optimal set of discrete parameters that can be used to characterize the solution to a problem. They use an evolutionary approach, mimicking the evolutionary processes in genetics. More specifically, an initial population of possible solutions (genes) is generated randomly, all with an associated fitness, reflecting the quality of the solution. These genes are then recombined using a crossover mechanism, which results in a future generation of the population, where genes with the highest fitness survive into later generations. This way, a genetic algorithm is more likely to efficiently locate a *global* minimum than calculus-based methods [42, 43]. The attractiveness of a genetic algorithm is in the simplicity of the implementation, which is taken one step further in this work by using the

default `ga.m` function in Matlab<sup>®</sup> with default options (all but for the initial population). The remainder of this section will elaborate on the genes that are used, the corresponding fitness, bounds, and constraints, as well as how the separate runs of the algorithm are set up.

As stated in the introduction of this section, several parameters have to be found: departure time ( $t_{dep}$ ), arrival time ( $t_{arr}$ ), time at linkage of the two CR3BPs ( $t_{link}$ ), and the orientation of the sail ( $\alpha$  and  $\delta$ ) over time. While the DST-technique assumes a constant sail orientation to limit the dimensions of the grid search, the genetic algorithm can easily accommodate a varying orientation over time, resulting in the following gene structure:

$$\mathbf{X} = \left[ t_{dep} \quad t_{arr} \quad t_{link} \quad \boldsymbol{\alpha}_1 \quad \boldsymbol{\delta}_1 \quad \boldsymbol{\alpha}_2 \quad \boldsymbol{\delta}_2 \right]^T, \quad (17)$$

where  $\boldsymbol{\alpha}_1$  and  $\boldsymbol{\delta}_1$  contain the set of cone and clock angles used in phase 1 (i.e., in the SE-CR3BP) and similarly for  $\boldsymbol{\alpha}_2$  and  $\boldsymbol{\delta}_2$  in phase 2 (i.e., in the Sun-planet CR3BP of the target planet). The different cone and clock angles are divided within each phase over  $n_{interval}$  equidistant time intervals. For this particular application, a value for  $n_{interval}$  of 3 is chosen, because tests show that both a lower value and a higher value result in more computation time for an equally feasible trajectory.

Bounds and constraints for the parameters in the gene structure of Eq. (17) are defined as follows:

- $t_{dep}$  can vary over one synodic Earth-planet period, again starting from 1-7-2020 for the Earth-Mars transfers 1-7-2021 and for the Earth-Venus transfers.
- $t_{arr}$  can vary such that  $t_{t_{min}} \leq t_t \leq t_{t_{max}}$ , which is enforced using a linear constraint.
- $t_{link}$  can vary between 25% and 75% of the total transfer time, which is also enforced using a linear constraint.
- $0^\circ \leq \boldsymbol{\alpha}_1, \boldsymbol{\alpha}_2 \leq 90^\circ$ .
- $-180^\circ \leq \boldsymbol{\delta}_1, \boldsymbol{\delta}_2 \leq 180^\circ$ .

Note that time is expressed in seconds since 1-1-2000 12:00 (noon), but in order to keep the bounds for the time-variables in the same order of magnitude as the bounds on  $\alpha$  and  $\delta$ , a scaling factor of  $10^{-8}$  has been applied, resulting in, for example, 18-7-2021 corresponding to  $t = 6.8$ . The use of this scaling factor shows improved performance of the genetic algorithm. Finally, instead of using the default initial population of the `ga.m` function, which is biased towards the boundaries of the parameters, the initial population is generated according to a pseudorandom uniform distribution between the defined bounds.

The fitness of each individual in the population is based on the discontinuities at linkage in the heliocentric inertial frame. These discontinuities ( $\Delta r$  in [km] and  $\Delta v$  in [km/s]) have to be expressed in one fitness value, for which a scaling factor,  $s_v$ , is used as follows:

$$J = \Delta r + s_v \Delta v. \quad (18)$$

This scaling factor is required because at linkage of the initial guess, a position discontinuity of multiple kilometers causes no convergence problems for the optimal control solver, but a velocity discontinuity of, for example, one kilometer per second or more is much harder to overcome by the optimal control solver.

The inherent randomness of genetic algorithms requires the algorithm described above to be run multiple times in order to increase the chance of locating the global minimum. In this work, the genetic algorithm has been initialized with 10 different seed values for the random number generator (RNG) as well as with different scaling factors of the fitness function,  $s_v$ . Trials runs show a suitable range of  $s_v$  for this application to lie between 10,000 and 700,000. The results for the HM-case can be found in Fig. 7. It can be seen that the position discontinuity is very small for all runs, which was also observed for the other three transfer cases. The final initial guess is therefore chosen based on the combination of the  $\Delta v$  at linkage and the transfer time,  $t_t$ , of which the results can be found in Table 5 for all cases, where all values for  $\alpha$  and  $\delta$  are given chronologically.

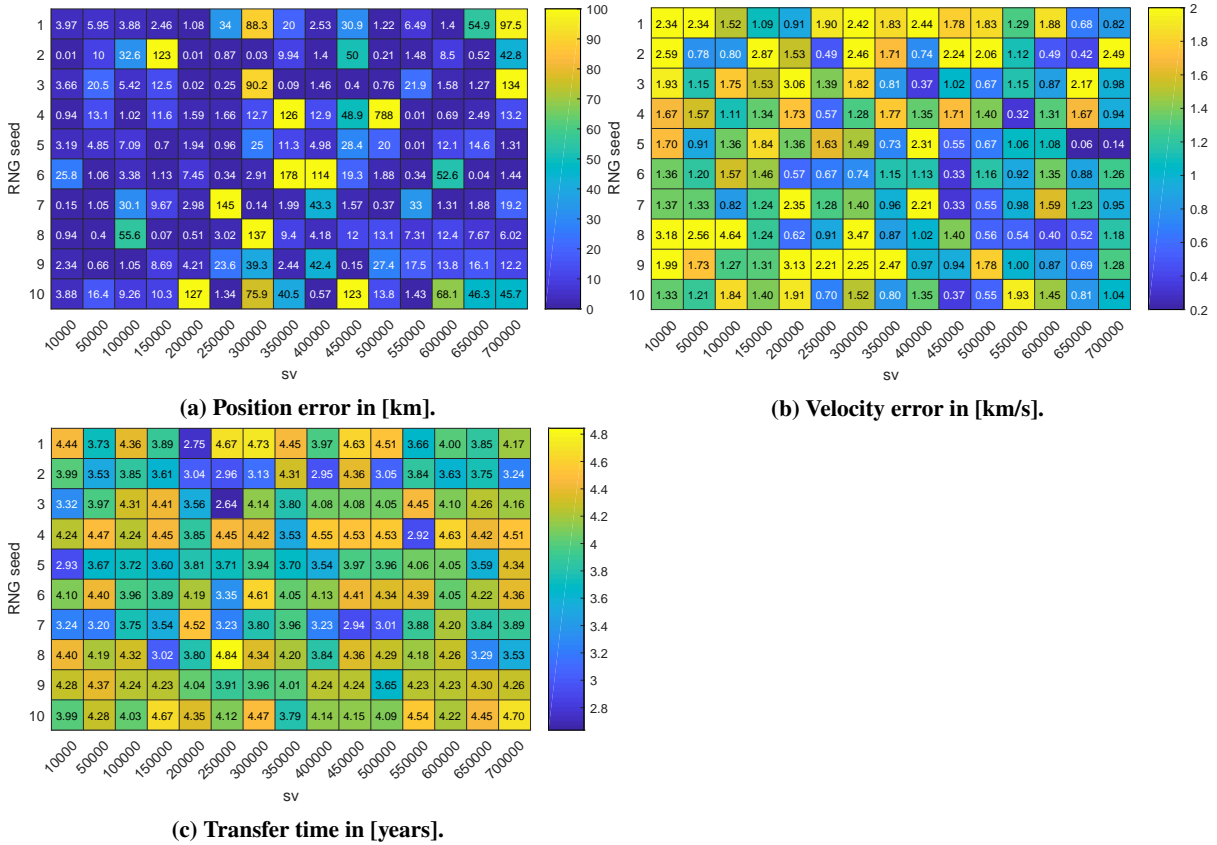


Fig. 7 Example genetic algorithm result HM pole-sitter transfer, for multiple scaling factors  $s_v$  (horizontal axis) and RNG seeds (vertical axis).

**Table 5 Initial guesses found using the genetic algorithm, along with the associated discontinuities at linkage, the transfer times, and the settings for the genetic algorithm.**

	HM	QM	HV	QV
$t_{dep}$	3-11-2021	29-10-2021	12-2-2021	19-4-2021
$t_{arr}$	5-10-2024	20-9-2024	26-7-2022	29-8-2022
$t_{link}$	24-4-2023	2-10-2023	23-4-2022	25-1-2022
$\alpha_1$ [deg]	[35.26, 47.11, 37.50]	[46.37, 33.37, 33.69]	[39.16, 69.18, 61.23]	[59.61, 55.53, 42.76]
$\delta_1$ [deg]	[93.43, 93.69, 101.18]	[105.49, 100.32, 103.22]	[-121.28, -94.49, -76.19]	[-97.16, -83.19, -55.70]
$\alpha_2$ [deg]	[46.86, 36.62, 46.49]	[45.85, 51.44, 50.12]	[42.62, 52.26, 29.32]	[53.26, 56.92, 53.20]
$\delta_2$ [deg]	[120.87, 91.34, 93.15]	[114.33, 64.21, 122.61]	[-107.5, -34.19, -84.82]	[-82.24, -95.4, -97.86]
$\Delta r$ [km]	0.0023134	0.18455	0.14954	0.023571
$\Delta v$ [km/s]	0.3218	0.41021	0.44787	0.58571
$t_t$ [years]	2.9217	2.8931	1.4488	1.3617
RNG seed	4	3	4	9
$s_v$	550,000	50,000	400,000	300,000

### C. Discussion on Initial Guess Solutions

Comparing the resulting initial guess solutions from Tables 4 and 5, many similarities can be observed. Note that it is not expected that both methods produce the exact same initial guess, because of the discrete approach of the DST-technique and the randomness of the genetic algorithm. The following is observed from Tables 4 and 5:

- 1) Very similar initial guesses are found for the (quasi-)pole-sitters at Mars, based on the dates of departure, arrival, and linkage, and the sail orientation. The initial guesses for the transfers to HM and QM also bear a remarkable resemblance, which can be explained by noting that a major portion of the transfer is dedicated to targeting Mars and only a small portion to targeting the (quasi-)pole-sitter itself.
- 2) Where the DST-technique assumes a fixed value for  $\delta$  at  $\pm 90^\circ$  (from [22, 23]), the genetic algorithm finds values different from  $\pm 90^\circ$ . This can be explained by the state at the SOI in the SE-CR3BP, which results from the Earth departure orbit in the Earth-centered inertial frame, which is tilted with respect to the ecliptic at an angle of  $23.44^\circ$ . Depending on the departure date, the initial condition in the SE-CR3BP can be inclined (up or down) with respect to the ecliptic, while the trajectory is more optimal in or close to the ecliptic. The velocity, and subsequently the position, in the out-of-plane direction is changed by a clock angle different from  $90^\circ$ , which is an explanation for the different clock angles observed in Tables 4 and 5. However, noting that the departure time can be anytime within the year, it is not advised to perform the analysis using the DST-technique with a clock angle different from  $\pm 90^\circ$ .
- 3) Another striking difference is that the genetic algorithm is able to find initial guesses with much smaller values for  $\Delta r$  than the DST-technique. This can be explained by, on the one hand, the discrete approach of the DST-technique, and on the other hand, the constant clock angle assumed in that technique. This builds upon the explanation provided in point 2) above, because the constant clock angle of  $\pm 90^\circ$  means that the sail is not able

to provide an acceleration in the out-of-plane direction.

It should be noted that for both the genetic algorithm and the DST-technique initial guesses were found with a smaller velocity discontinuity, but that these transfers took much longer than the initial guesses that were selected, and were therefore considered less favorable.

Besides the quality of the initial guesses, where the genetic algorithm produces smaller discontinuities, several other elements have to be addressed in order to compare the two methods. One element is the computation time required to perform the analysis, which can be found in Table 6. Note that the computation time is of course highly dependent on the written code. However, both techniques are coded in Matlab<sup>®</sup>, using the same dynamical model and following the same basic principle (forward and backward propagation of the initial and final state and comparing at linkage). Also, both algorithms have been optimized using Matlab<sup>®</sup>'s profiler, minimizing the computation time. Because of these reasons, the computational time can, at least qualitatively, be compared. Table 6 shows that the genetic algorithm clearly outperforms the DST-technique, by 22.7% - 36.5% in computation time.

In addition, as no a-priori decisions have to be made (e.g. on the clock angle or on a suitable range for the cone angle), the genetic algorithm is easier to implement without requiring a detailed understanding of the dynamical model and the problem, while resulting in more feasible initial guesses.

**Table 6 Total computation time in [hh:mm] using Intel Xeon processors (type E5-2683 v3.0) with a clock speed of 2.0 GHz per thread. Computation time is the sum over all threads.**

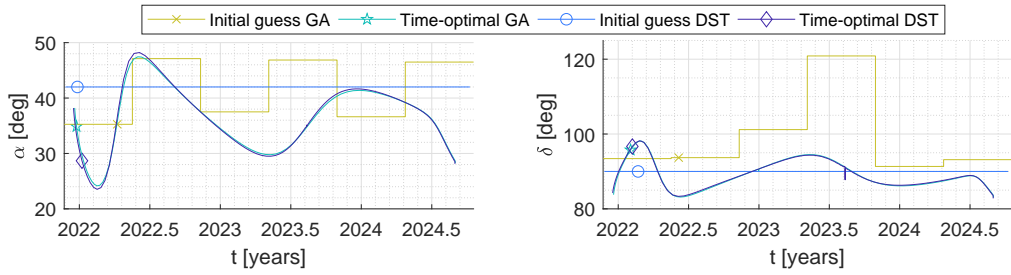
	HM	QM	HV	QV
DST-technique	153:39	157:11	162:23	159:06
Genetic algorithm	118:46	114:34	123:09	101:05
Difference in computation time genetic algorithm w.r.t DST-technique	-22.7 %	-27.1 %	-24.2 %	-36.5 %

## VI. Results

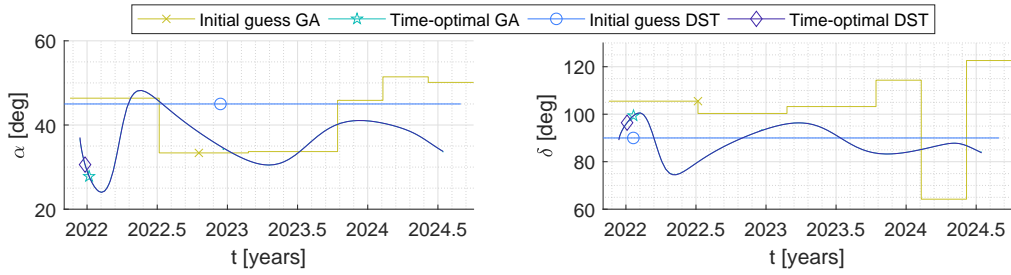
The initial guesses tabulated in Tables 4 and 5 are all separately optimized using PSOPT, conform the optimal control problem defined in Section III. The resulting range of time-optimal results is presented in this section.

First, the control profiles for the time-optimal transfers, along with those for the initial guesses, are provided in Fig. 8 for both Mars (quasi-)pole-sitters and in Fig. 9 for both Venus (quasi-)pole-sitters. The resulting range of values for the cone angle, as well as the trend observed in Figs. 8 and 9 are in good agreement with References [23, 44, 45].

Subsequently, the transfer times are summarized in Table 7 for all time-optimal transfers. From the table, as well as from Fig. 8 and 9, it can be seen that the two time-optimal transfers (for the DST- and GA- initial guesses) are very similar for each case. Nonetheless, comparing the resulting transfer times results in a difference of less than two days for the HM case, and within hours for the QM, HV, and QV cases. The transfer with the shortest transfer time is considered most optimal and denoted in boldface in Table 7.

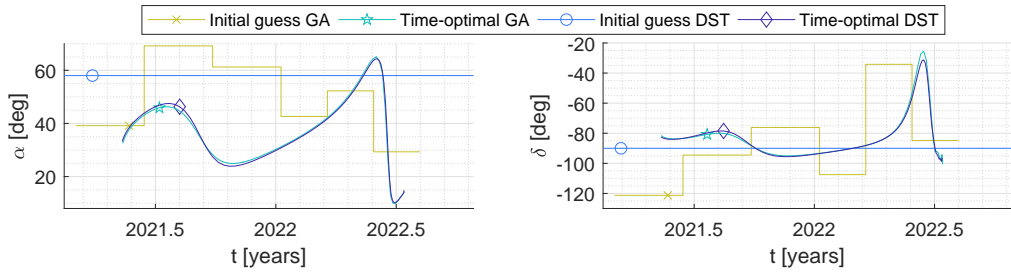


(a) Case HM.

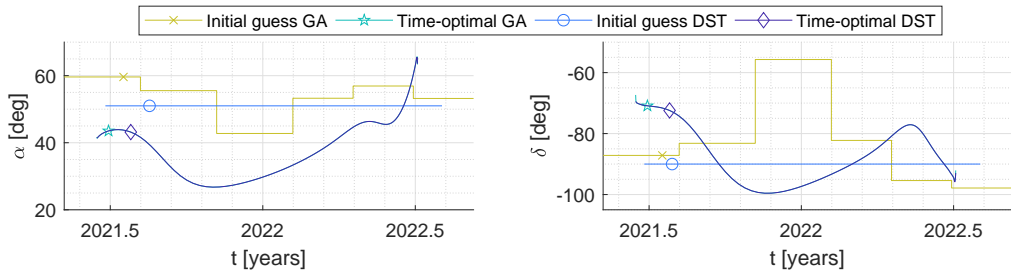


(b) Case QM.

**Fig. 8 Initial guesses and time-optimal control profiles for the Mars (quasi-)pole-sitters.**



(a) Case HV.



(b) Case QV.

**Fig. 9 Initial guesses and time-optimal control profiles for the Venus (quasi-)pole-sitters.**

**Table 7** Departure and arrival dates, as well as transfer times, for all time-optimal transfers.

		HM	QM	HV	QV
DST-technique	Departure date	27-11-2021	24-11-2021	24-4-2021	28-5-2021
	Arrival date	18-8-2024	3-7-2024	2-7-2022	23-6-2022
	Transfer time [years]	2.72365	<b>2.60660</b>	1.18959	1.07112
Genetic algorithm	Departure date	30-11-2021	24-11-2021	24-4-2021	28-5-2021
	Arrival date	19-8-2024	3-7-2024	3-7-2022	23-6-2022
	Transfer time [years]	<b>2.71830</b>	2.60661	<b>1.18934</b>	<b>1.07111</b>

Furthermore, the most optimal transfers are shown in the heliocentric inertial frame in Fig. 10 for all cases. In addition, a 3D view in the heliocentric inertial frame of the transfer to HV is given in Fig. 11, showing the substantial out-of-plane solar sail acceleration. In both figures, the solar sail induced acceleration is shown using arrows, where the size of the arrow indicates the relative acceleration magnitude. It can be seen that the magnitude of the acceleration decreases when the sail spirals outwards, and increases when the sail spirals inwards, as expected. More detailed plots on the transfers to HM and HV are given in Fig. 12, including the departure from the GTO, the trajectories in the separate phases, and arrival at the pole-sitters. Note that the difference observed in the plots concerning the departure in the SE-CR3BP (subfigures a and e) is due to the different orientation of the equator with respect to the ecliptic over time, as discussed in Section V.C. In Fig. 12 (subfigures d and h), it can be seen that arrival at the pole-sitters occurs at the point closest to the planet, as is also the case for the quasi-pole-sitters. This is congruent with results from Reference [21], where a transfer to a pole-sitter at Earth is optimized.

Finally, recall from Section IV that in PSOPT, the state and controls are approximated at and between the collocation points using Legendre polynomials. In order to assess whether or not this is sufficiently accurate, the trajectory is reintegrated using the `ode45.m` integrator in Matlab<sup>®</sup>, an explicit Dormand-Prince method of order 4 with an adaptive stepsize, with relative and absolute tolerances of  $10^{-11}$ . The controls and time at the Legendre-Gauss-Lobatto nodes as provided by PSOPT are interpolated using a cubic spline, thereby increasing the number of collocation points by a factor of 1000, creating a near-continuous control profile. Forward propagating the initial state for the time-optimal transfer to HM, using the corresponding control profile, results in a 5068.3 km position discontinuity and 0.00099443 km/s velocity discontinuity at the pole-sitter. Note that this is equal to  $2.2235 \cdot 10^{-5}$  (position) and  $4.1210 \cdot 10^{-5}$  (velocity) in non-dimensional SM-CR3BP units, which is considered sufficiently accurate for this application.

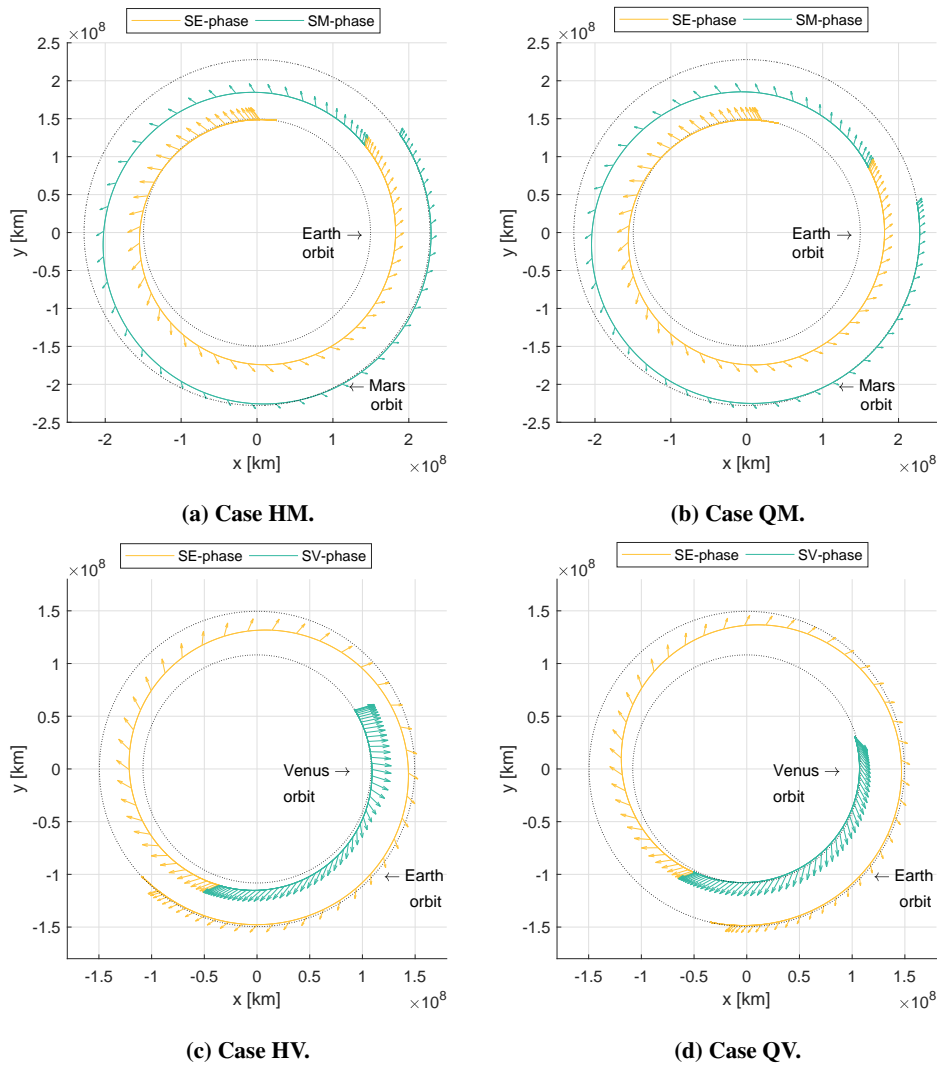


**Fig. 10** Most optimal transfers in the heliocentric inertial frame for all considered cases. Arrows indicate the solar sail induced acceleration. Note that, during the escape trajectory within Earth's SOI, no solar sail is employed (i.e., no arrows).

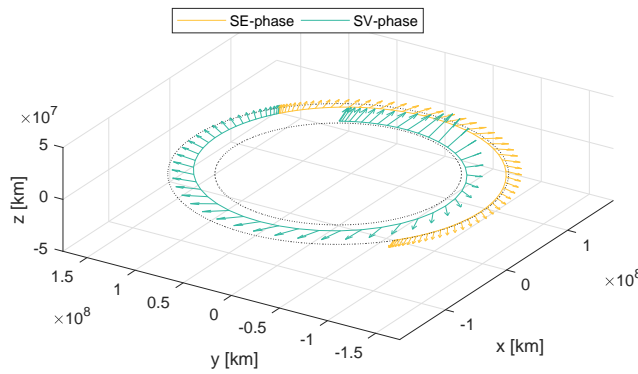


**Fig. 11** 3D view of the time-optimal transfer to the HV pole-sitter in the heliocentric inertial frame.

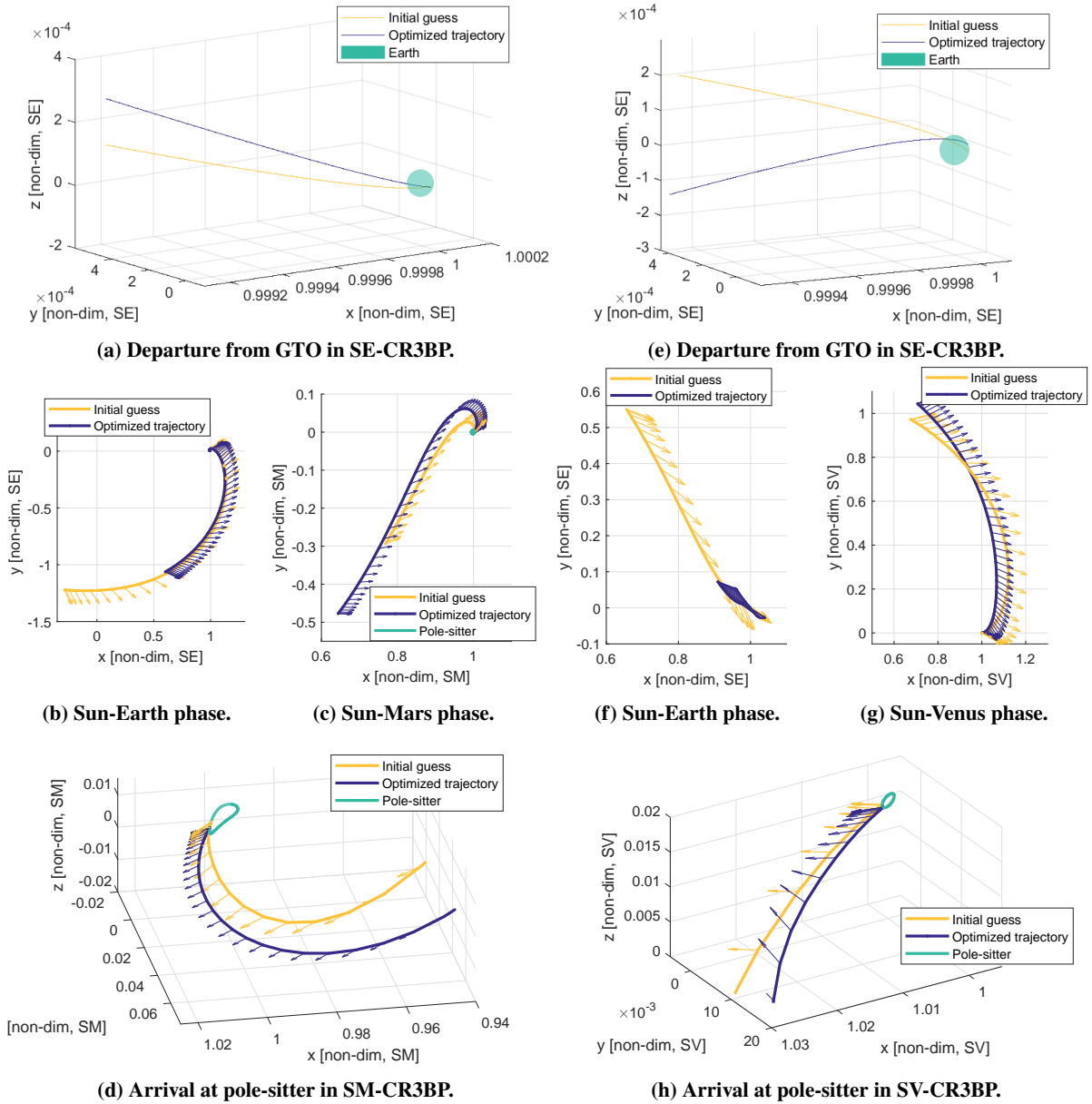


**Fig. 12** Detailed plots of time-optimal transfers to HM (a-d) and HV (e-h). Both the initial guess and time-optimal trajectory are shown. Arrows indicate the sail normal vector (note: not the acceleration).

## VII. Sensitivity Analyses

The previous sections have been carried out in compliance with the assumptions listed at the start of Section III:

- 1) The lightness number,  $\beta$ , is assumed to be equal to that for a near- to mid-term sail: 0.05 (for HM/QM/HV) and 0.06 (for QV, which is the minimum value for  $\beta$  required for a sail-only quasi-pole-sitter at Venus).
- 2) An ideal sail model is adopted, which assumes that *all* incoming radiation is perfectly reflected.
- 3) The departure orbit at Earth is a midnight-GTO, which assumes perigee to be on the night-side of the Earth on the Sun-planet line.

This section shows the impact of those assumptions for the HM case, where they will be treated separately.

### A. Lightness Number

Whereas a value for  $\beta$  of 0.05 is consistent with near- to mid-term solar sail technology, mid- to far-term solar sails are expected to achieve values for  $\beta$  up to 0.1 [29]. It is therefore interesting to see how the time-optimal transfers change for larger values for  $\beta$ . In addition, to make the pole-sitter concept feasible for current sail technology, the effect of a smaller value for  $\beta$  is considered as well. Note that this requires other hybrid Mars pole-sitters from Reference [15] to be considered, consistent with each value for  $\beta$ , even though this constitutes only a marginal change in final conditions.

Figure 13 shows the resulting control profile for this sensitivity analysis, as well as the accompanying transfer time. It can be seen that, as expected, for larger values for  $\beta$ , the transfer time decreases. Similarly, an increase in transfer times is visible for a smaller value for  $\beta$ . In fact, a nearly inversely proportional relationship is observed between the lightness number and the transfer time for the range of  $\beta$  values considered. For example, using mid- to far-term sail technology, with  $\beta = 0.1$ , a decrease in transfer time of 48.6% is observed with respect to the baseline result of  $\beta = 0.05$ .

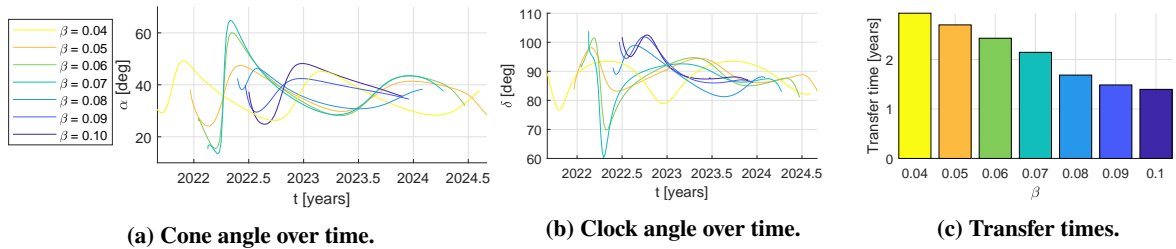


Fig. 13 Sensitivity analysis for changing lightness number for the HM pole-sitter.

### B. Optical Sail

Instead of assuming a perfectly reflecting sail, the higher fidelity, optical sail model is adopted in this section, see Section II.B. The optical sail will be introduced stepwise, by linearly interpolating the optical coefficients presented in

Table 2, between values equivalent to an ideal sail and the values given in Table 2. An ideal sail can be modeled using the dynamics for an optical sail, provided that  $\tilde{r} = s = 1$ ,  $B_b = B_f = \frac{2}{3}$ , and  $\epsilon_b = \epsilon_f = 10^{-16}$  (to avoid dividing by zero in the dynamical model) [1]. Figure 14 shows the control profiles for each step that was taken to introduce the optical sail parameters, where step 0 is consistent with an ideal sail, and step 4 the optical sail with coefficients equal to those provided in Table 2.

It can be seen in Fig. 14 that, as a result of the higher-fidelity sail model, the transfer time increases from 2.7183 years to 3.0130 years, which is equal to a 10.8% increase. This is consistent with results found in Reference [45], where an Earth-Mars rendezvous mission is optimized for minimum time both for an ideal and an optical sail (albeit with outdated optical sail coefficients and using  $\beta = 0.17$ ). In that work, an increase of 9.8% in the transfer time is observed. In Reference [10], an ideal sail model is compared to a realistic sail model, for a mission from a midnight-GTO to the sub- $L_1$  region in the Sun-Earth system, using  $\beta = 0.0363$ . Results obtained in that work show an 8.0% increase in transfer time. Because the influence of employing an optical sail rather than an ideal sail on the transfer time is dependent on the lightness number and type of trajectory, both results are considered comparable to the increase observed in this work. In addition, by comparing the control profiles of the time-optimal transfers using an ideal and optical sail model, it can be concluded that the non-ideal sail properties cause the control profile for the cone angle to be more flattened out, in other words, vary less over time.

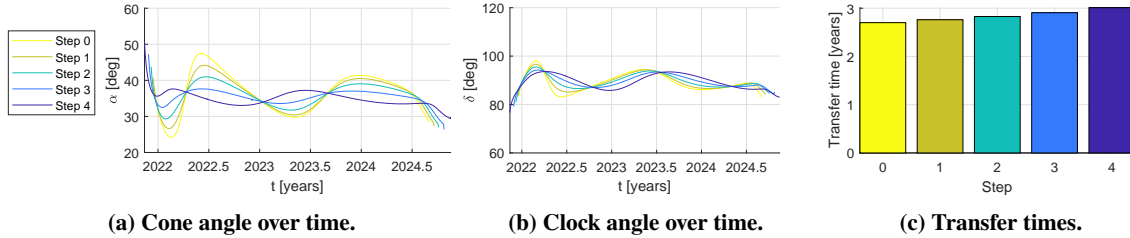


**Fig. 14 Sensitivity analysis for optical sail properties for the HM pole-sitter.**

### C. Earth Departure Orbit

The third and last assumption deals with the departure orbit at Earth, which is assumed to be a midnight-GTO, as explained in Section III.B. This assumption eliminates one optimization parameter, but inherently restricts the optimization. Therefore, the opposite extreme is also implemented: a midday-GTO, where perigee of the GTO is at the *day-side* of the Earth, on the Sun-Earth line.

Since the transfers to Mars and Venus spiral inwards and outwards, respectively, this assumption can have different effects on the transfers to the two planets. Therefore, this analysis is not only carried out for the HM case, but also for the HV case. The results can be found in Table 8. Table 8 shows that the effect of the GTO's orientation is indeed opposite for transfers to Mars and Venus, with a decrease in transfer time for the HM case of 4.1% and an increase in

transfer time for the HV case of 12.4%. From these results, it can be deduced that the most favorable departure orbit is one where perigee is on the day-side for transfers spiraling outwards (i.e., to Mars) and on the night-side for transfers spiraling inwards (i.e., to Venus).

**Table 8 Sensitivity analysis for departure orbit at Earth for the HM and HV pole-sitters.**

	HM		HV	
	Midnight-GTO	Midday-GTO	Midnight-GTO	Midday-GTO
Departure date	30-11-2021	7-12-2021	24-4-2021	20-1-2021
Arrival date	19-8-2024	23-8-2024	3-7-2022	29-6-2022
Transfer time [years]	2.7183	2.6075	1.1893	1.3367

## VIII. Conclusion

In this paper, time-optimal solar sail trajectories from a midnight-GTO to (quasi-)pole-sitters at Mars and Venus have been investigated. In particular, transfers to hybrid pole-sitters and quasi-pole-sitters at Mars and Venus that are achievable with near- to mid-term solar sail technology (lightness number of 0.05 or 0.06) have been considered.

To solve the optical control problem a direct pseudospectral optimal control solver has been employed in this work. Since optimal control solvers are known to be sensitive to the provided initial guess, initial guesses were generated through two completely different methods. On the one hand, a robust method that is proven for these kinds of transfers is used, which is based on a technique from dynamical systems theory, where connections of invariant manifolds are sought for. On the other hand, a genetic algorithm is employed, which requires no a-priori knowledge and is simple to implement. While the resulting initial guesses show comparable departure and arrival dates and sail orientations, the genetic algorithm provides slightly more feasible initial guesses. In addition, the genetic algorithm outperforms the technique from dynamical systems theory based on computation time and ease of implementation. Subsequent optimization of the initial guesses results in remarkably similar time-optimal results, that are within a two day difference in transfer time for all considered cases, thereby validating the obtained initial guesses. In particular, the time-optimal transfers require 2.718 years for the case considering the hybrid pole-sitter at Mars, 2.607 years for the quasi-pole-sitter at Mars, 1.190 years for the hybrid pole-sitter at Venus, and 1.071 years for the quasi-pole-sitter at Venus. Note that these transfers depart from a parabolic escape trajectory, for which a  $\Delta v$  of 0.7693 km/s at GTO's perigee is required. Additionally, a range of sensitivity analyses has been performed. First, it is shown that using mid- to far-term solar sail technology (lightness number of 0.1), the transfer time can decrease significantly, up to a 48.6% decrease for the hybrid pole-sitter at Mars. Furthermore, using an optical sail model rather than a perfectly reflecting sail model, a modest increase of 10.8% of the transfer time is observed. Finally, departing from a midday-GTO instead of a midnight-GTO, results in a decrease of 4.1% for the transfer time to the hybrid pole-sitter at Mars, and a 12.4% increase for the hybrid pole-sitter at Venus.

Since the two initial guess techniques both produce near-feasible and comparable solutions, the two design approaches are both validated. However, in terms of computational time, ease of implementation, and feasibility of the initial guess, the genetic algorithm outperforms the technique from dynamical systems theory and is therefore recommended.

## Appendix: Reference Frame Transformations

### A. Sun-Planet CR3BP to Heliocentric Inertial Frame

This section describes the transformation from the Sun-planet synodic frame,  $A(\hat{\mathbf{x}}, \hat{\mathbf{y}}, \hat{\mathbf{z}})$  (with  $\mathbf{x} = \begin{bmatrix} \mathbf{r} & \dot{\mathbf{r}} \end{bmatrix}$ ), to a heliocentric inertial frame,  $H(\hat{\tilde{\mathbf{X}}}, \hat{\tilde{\mathbf{Y}}}, \hat{\tilde{\mathbf{Z}}})$  (with  $\tilde{\mathbf{X}} = \begin{bmatrix} \tilde{\mathbf{R}} & \dot{\tilde{\mathbf{R}}} \end{bmatrix}$ ).

The first step is to translate the barycenter of the Sun-planet CR3BP to the center of the Sun:

$$\mathbf{r}' = \mathbf{r} + \begin{bmatrix} \mu & 0 & 0 \end{bmatrix}^T, \quad (19)$$

after which the state and time are dimensionalized (denoted by a tilde) using the variables from Table 1. Then,

$$\tilde{\mathbf{R}} = \mathbb{T}_z(\phi)\tilde{\mathbf{r}}', \quad (20a)$$

$$\dot{\tilde{\mathbf{R}}} = \mathbb{T}_z(\phi)(\dot{\tilde{\mathbf{r}}} + \boldsymbol{\omega} \times \tilde{\mathbf{r}}'), \quad (20b)$$

where  $\mathbb{T}_z$  is the rotation matrix around the  $\hat{\mathbf{z}}$ -axis and  $\phi$  the angle in radians between the Sun-planet line and the vernal equinox, calculated by:

$$\phi = \phi_0 + t, \quad (21)$$

where  $t$  is the non-dimensional time, as discussed in Section A, and  $\phi_0$  the initial angle in radians between the Sun-planet line and the vernal equinox at  $t = 0$ , corresponding to 1-1-2000 12:00 (noon), see Table 9.

**Table 9 Initial angle between Sun-planet line and vernal equinox. The value for  $\phi_0$  is based on data from the NASA/JPL Horizons online ephemeris system [46].**

	SE-CR3BP	SM-CR3BP	SV-CR3BP
$\phi_0$ [deg]	100.307	-0.986	-178.004

## B. Heliocentric Inertial Frame to Sun-Planet CR3BP

The reverse of the transformation in the previous section is performed as follows. First:

$$\tilde{\mathbf{r}}' = \mathbb{T}_z(-\phi)\tilde{\mathbf{R}}, \quad (22a)$$

$$\dot{\tilde{\mathbf{r}}}' = \mathbb{T}_z(-\phi)\left(\dot{\tilde{\mathbf{R}}} - \boldsymbol{\omega} \times \tilde{\mathbf{R}}\right), \quad (22b)$$

after which the state and time are non-dimensionalized using the units of the target CR3BP from Table 1, and

$$\mathbf{r} = \mathbf{r}' - \begin{bmatrix} \mu & 0 & 0 \end{bmatrix}^T. \quad (23)$$

## C. Cartesian Earth-Centered Inertial Frame to SE-CR3BP

The transformation from the Cartesian Earth-centered inertial frame (with  $\tilde{\mathbf{X}}_E = \begin{bmatrix} \tilde{\mathbf{R}}_E & \dot{\tilde{\mathbf{R}}}_E \end{bmatrix}$ ) to the SE-CR3BP (with  $\mathbf{x} = \begin{bmatrix} \mathbf{r} & \dot{\mathbf{r}} \end{bmatrix}$ ) starts with a rotation around the  $\hat{\mathbf{X}}_E$ -axis over the obliquity of the ecliptic,  $\delta_{eq}$ :

$$\tilde{\mathbf{R}}'_E = \mathbb{T}_x(-\delta_{eq})\tilde{\mathbf{R}}_E, \quad (24a)$$

$$\dot{\tilde{\mathbf{R}}}'_E = \mathbb{T}_x(-\delta_{eq})\dot{\tilde{\mathbf{R}}}_E, \quad (24b)$$

where  $\mathbb{T}_x$  is the rotation matrix around the  $\hat{\mathbf{X}}_E$ -axis. Next, the state and time are non-dimensionalized using the units of the SE-CR3BP from Table 1. Then,

$$\tilde{\mathbf{r}}' = \mathbb{T}_z(-\phi)\mathbf{R}'_E, \quad (25a)$$

$$\dot{\tilde{\mathbf{r}}}' = \mathbb{T}_z(-\phi)\left(\dot{\mathbf{R}}'_E - \boldsymbol{\omega} \times \mathbf{R}'_E\right). \quad (25b)$$

And finally,

$$\mathbf{r} = \mathbf{r}' + \begin{bmatrix} (1 - \mu) & 0 & 0 \end{bmatrix}^T. \quad (26)$$

## References

- [1] McInnes, C. R., *Solar sailing: technology, dynamics and mission applications.*, Springer-Praxis series in space science and technology, Berlin, 1999.
- [2] Tsuda, Y., Mori, O., Funase, R., Sawada, H., Yamamoto, T., Saiki, T., Endo, T., and Kawaguchi, J., “Flight status of IKAROS deep space solar sail demonstrator,” *Acta Astronautica*, Vol. 69, No. 910, 2011, pp. 833 – 840. doi:10.1016/j.actaastro.2011.06.005.

- [3] Johnson, L., Whorton, M., Heaton, A., Pinson, R., Laue, G., and Adams, C., “NanoSail-D: A solar sail demonstration mission,” *Acta Astronautica*, Vol. 68, No. 56, 2011, pp. 571–575. doi:10.1016/j.actaastro.2010.02.008, special Issue: Aosta 2009 Symposium.
- [4] Bidy, C., and Svitek, T., “LightSail-1 Solar Sail Design and Qualification,” *Proceedings of the 41st Aerospace Mechanisms Symposium, Jet Propulsion Laboratory, May 16-18, 2012*, 2012.
- [5] McKay, R. J., Macdonald, M., Biggs, J., and McInnes, C. R., “Survey of Highly-Non-Keplerian Orbits with Low-Thrust Propulsion,” *Journal of Guidance, Control and Dynamics*, Vol. 34, No. 3, 2011, pp. 645 – 666. doi:10.2514/1.52133.
- [6] Heiligers, J., Macdonald, M., and Parker, J. S., “Extension of Earth-Moon Libration Point Orbits with Solar Sail Propulsion,” *Astrophysics and Space Science*, Vol. 361, No. 7, 2016. doi:10.1007/s10509-016-2783-3.
- [7] Heiligers, J., Hiddink, S., Noomen, R., and McInnes, C. R., “Solar sail Lyapunov and Halo orbits in the Earth–Moon three-body problem,” *Acta Astronautica*, Vol. 116, 2015, pp. 25–35. doi:10.1016/j.actaastro.2015.05.034.
- [8] Ceriotti, M., Diedrich, B. L., and McInnes, C. R., “Novel mission concepts for polar coverage: An overview of recent developments and possible future applications,” *Acta Astronautica*, Vol. 80, 2012, pp. 89 – 104.
- [9] Macdonald, M., and McInnes, C., *Solar sail science mission applications and advancement*, Vol. 48, Elsevier BV, 2011. doi:10.1016/j.asr.2011.03.018.
- [10] Heiligers, J., Diedrich, B., Derbes, B., and McInnes, C. R., “Sunjammer: Preliminary end-to-end mission design.” *AIAA/AAS Astrodynamics Specialist Conference 2014*, 2014.
- [11] Heiligers, J., and McInnes, C. R., “Novel Solar Sail Mission Concepts for Space Weather Forecasting,” *24th AAS/AIAA Space Flight Mechanics Meeting, Santa Fe, NM*, 2014.
- [12] McInnes, C., Bothmer, V., Dachwald, B., Geppert, U., Heiligers, J., Hilgers, A., Johnson, L., Macdonald, M., Reinhard, R., Seboldt, W., and Spietz, P., *Advances in Solar Sailing*, Springer Berlin Heidelberg, 2014, Chaps. Gossamer Roadmap Technology Reference Study for a Sub-L1 Space Weather Mission, pp. 227–242.
- [13] Macdonald, M., Hughes, G., McInnes, C., Lyngvi, A., and Alessandro Atzei, P. F., “Solar Polar Orbiter: A Solar Sail Technology Reference Study Read More: <https://arc.aiaa.org/doi/abs/10.2514/1.16408>,” *Journal of Spacecraft and Rockets*, Vol. 43, No. 5, 2006, pp. 960–972. doi:10.2514/1.16408.
- [14] Ceriotti, M., Heiligers, J., and McInnes, C. R., “Trajectory and spacecraft design for a pole-sitter mission,” *Journal of Spacecraft and Rockets*, Vol. 51, No. 1, 2014, pp. 311–326.
- [15] Heiligers, J., van den Oever, T. D., Ceriotti, M., Mulligan, P., and McInnes, C. R., “Continuous Planetary Polar Observation from Hybrid Pole-Sitters at Venus, Earth, and Mars,” *Fourth International Symposium on Solar Sailing (ISSS 2017), Kyoto, Japan, 17-20 Jan 2017*, 2016.

- [16] McInnes, C. R., and Mulligan, P., “Final Report: Telecommunications and Earth Observations Applications for Polar Stationary Solar Sails,” , 2003. Report to the National Oceanic and Atmospheric Administration from the Department of Aerospace Engineering, University of Glasgow.
- [17] Ceriotti, M., and McInnes, C. R., “Generation of optimal trajectories for Earth hybrid pole sitters,” *Journal of Guidance, Control, and Dynamics*, Vol. 34, No. 3, 2011, pp. 847–859.
- [18] Ceriotti, M., and McInnes, C. R., “Hybrid solar sail and solar electric propulsion for novel Earth observation missions,” *Acta Astronautica*, Vol. 69, No. 9-10, 2011, pp. 809–821. doi:10.1016/j.actaastro.2011.06.007.
- [19] Leipold, M., and Götz, M., “Hybrid Photonic/Electric Propulsion,” , January 2002. Rept. SOL4- TR-KTH-0001.
- [20] Walmsley, M., Heiligers, J., Ceriotti, M., and McInnes, C. R., “Optimal Trajectories for Planetary Pole-Sitter Missions,” *Journal of Guidance, Control and Dynamics*, 2016. Accepted for publication.
- [21] Heiligers, J., Ceriotti, M., McInnes, C. R., and Biggs, J. D., “Design of optimal Earth pole-sitter transfers using low-thrust propulsion,” *Acta Astronautica*, Vol. 79, 2012, pp. 253–268.
- [22] Mingotti, G., Heiligers, J., and McInnes, C. R., “First-guess generation of solar sail Interplanetary heteroclinic connections,” *2nd IAA Conference on Dynamics and Control of Space Systems, Rome, Italy*, 2014.
- [23] Vergaaij, M., and Heiligers, J., “Time-Optimal Solar Sail Heteroclinic Connections for an Earth-Mars Cyclers,” *68th International Astronautical Congress, Adelaide, Australia, 25-29 September, 2017*, 2017.
- [24] Becerra, V. M., “Solving complex optimal control problem at no cost with PSOPT,” *IEEE International Symposium on Computer-Aided Control System Design, Yokohama, Japan, 7-10 September*, 2010. doi:10.1109/CACSD.2010.5612676.
- [25] Battin, R. H., *An Introduction to the Mathematics and Methods of Astrodynamics, Revised Edition*, AIAA Education Series, American Institute of Aeronautics & Astronautics, Reston, VA, 1999.
- [26] Szebehely, V., *Theory of Orbits: The Restricted Problem of Three Bodies*, Academic Press Inc., New York, 1967.
- [27] Baig, S., and McInnes, C. R., “Artificial three-body equilibria for hybrid low-thrust propulsion,” *Journal of Guidance, Control, and Dynamics*, Vol. 31, No. 6, 2008, pp. 1644–1655.
- [28] Dachwald, B., Mengali, G., Quarta, A., and Macdonald, M., “Parametric model and optimal control of solar sails with optical degradation,” *Journal of Guidance, Control, and Dynamics*, Vol. 29, No. 5, 2006, pp. 1170–1178. doi:10.2514/1.20313.
- [29] Ceriotti, M., and McInnes, C. R., “Systems design of a hybrid sail pole-sitter,” *Advances in Space Research*, Vol. 48, No. 11, 2011, pp. 1754–1762.
- [30] Heaton, A., Ahmad, N., and Miller, K., “Near Earth Asteroid Scout Solar Sail Thrust and Torque Model,” *4th International Symposium on Solar Sailing (ISSS 2017), 17-20 Jan. 2017, Kyoto, Japan*, 2017.

- [31] Scheeres, D. J., *Orbital Motion in Strongly Perturbed Environments*, Springer Berlin Heidelberg, 2012. doi:10.1007/978-3-642-03256-1.
- [32] Ariespace, *Ariane V User's Manual, Issue 5, Edition 1*, 2011.
- [33] Bate, R., Mueller, D., and White, J., *Fundamentals of Astrodynamics*, Dover Publications, New Academic Press Inc., New York, 1971.
- [34] Wächter, A., and Biegler, L., "On the Implementation of a Primal-Dual Interior Point Filter Line Search Algorithm for Large-Scale Nonlinear Programming," *Mathematical Programming*, Vol. 106, No. 1, 2006, pp. 25–57.
- [35] Rao, A., "A Survey of Numerical Methods for Optimal Control," *Advances in the Astronautical Sciences*, Vol. 135, No. 1, 2009, p. 4. doi:10.1.1.661.6337.
- [36] Cage, P., Kroo, I., and Braun, R., "Interplanetary trajectory optimization using a genetic algorithm," *Astrodynamics Conference*, American Institute of Aeronautics and Astronautics, 1994. doi:10.2514/6.1994-3773.
- [37] Rauwolf, G. A., and Coverstone-Carroll, V. L., "Near-optimal low-thrust orbit transfers generated by a genetic algorithm," *Journal of Spacecraft and Rockets*, Vol. 33, No. 6, 1996, pp. 859–862. doi:10.2514/3.26850.
- [38] Wall, B., and Conway, B. A., "Near-Optimal Low-Thrust Earth-Mars Trajectories via a Genetic Algorithm," *Journal of Guidance, Control, and Dynamics*, Vol. 28, No. 5, 2005, pp. 1027–1031. doi:10.2514/1.11891.
- [39] Williams, S., Hartmann, J., and Coverstone-Carroll, V., "Optimal Interplanetary Spacecraft Trajectories via a Pareto Genetic Algorithm," *Spaceflight Mechanics*, 1998.
- [40] Coverstone-Carroll, V., Hartmann, J., and Mason, W., "Optimal multi-objective low-thrust spacecraft trajectories," *Computer Methods in Applied Mechanics and Engineering*, Vol. 186, No. 2-4, 2000, pp. 387–402. doi:10.1016/s0045-7825(99)00393-x.
- [41] Dachwald, B., "Evolutionary neurocontrol: A smart method for global optimization of low-thrust trajectories," *Collection of Technical Papers - AIAA/AAS Astrodynamics Specialist Conference*, Vol. 3, 2004, pp. 1705–1720.
- [42] Goldberg, D. E., *Genetic Algorithms in Search, Optimization, and Machine Learning*, Addison-Wesley Publishing Company, Inc., 1989.
- [43] Conway, B. A., *Spacecraft Trajectory Optimization*, Cambridge Aerospace Series, American Institute of Aeronautics and Astronautics, Cambridge, 2010.
- [44] Heiligers, J., Mingotti, G., and McInnes, C. R., "Optimal solar sail transfers between halo orbits of different Sun-planet systems," *Advances in Space Research*, Vol. 55, No. 5, 2015, pp. 1405–1421.
- [45] Mengali, G., and Quarta, A. A., "Solar sail trajectories with piecewise-constant steering laws," *Aerospace Science and Technology*, Vol. 13, No. 8, 2009, pp. 431–441. doi:10.1016/j.ast.2009.06.007.
- [46] NASA, Jet Propulsion Laboratory, "HORIZONS Web-Interface," <https://ssd.jpl.nasa.gov/horizons.cgi>, Accessed on: June 21, 2017, 2017.



# 3

## Conclusions and Recommendations

In this thesis, time-optimal solar sail transfers to various (quasi-)pole-sitters at Mars and Venus have been investigated. The purpose of this was twofold: on the one hand, to demonstrate the feasibility of the (quasi-)pole-sitter mission concept, while on the other hand, to assess and compare two initial guess techniques, in order to see which one is more suitable for this particular problem. This chapter will conclude this thesis report, starting with the answers to all research (sub)questions posed in Section 3.1, followed by the recommendations for future work in Section 3.2, and finally, in Section 3.3, the implications of this work will be set out.

### 3.1. Conclusions

The research questions for this thesis work were structured into two separate main research questions, each with a number of associated research subquestions. In this section, answers to the research question and subquestions will be provided separately.

**1. What is the minimum time of flight for a transfer from a departure orbit at Earth to a hybrid- or quasi-pole-sitter position at Mars or Venus when employing solar sailing as a means of propulsion?**

The transfers have been designed using the following assumptions: an ideal sail is employed, with a lightness number of  $\beta = 0.05$  (for transfers to both the hybrid and the quasi-pole-sitter at Mars and the hybrid pole-sitter at Venus) or 0.06 (for the transfer to the quasi-pole-sitter at Venus), and the departure orbit is a midnight-GTO. Under these assumptions, the transfer to the hybrid pole-sitter at Mars spans 2.718 years, slightly more than the transfer to the quasi-pole-sitter at Mars, which spans 2.607 years. The control profiles for these time-optimal transfers are very similar, because a major portion of the transfer is dedicated to targeting Mars and only a small portion to targeting the (quasi-)pole-sitter itself. The minor difference in transfer time is attributed to the fact that the quasi-pole-sitter is located closer to the Sun and therefore closer to the Earth. The transfer to the hybrid pole-sitter at Venus spans 1.190 years, while the transfer to the quasi-pole-sitter at Venus spans 1.071 years. While the transfer to the quasi-pole-sitter is designed using a higher lightness number, resulting in a shorter transfer time, the quasi-pole-sitter is located closer to the Sun than the hybrid pole-sitter (thus farther away from the Earth), which in turns causes a slight increase in transfer time.

**(a) What is the effect of including optical imperfections in the solar sail model on the minimum-time transfer?**

In order to answer this subquestion, a sensitivity analysis has been performed for the transfer to the hybrid pole-sitter at Mars. Instead of assuming a perfectly reflecting (i.e., ideal) sail, an optical sail model has been implemented, which incorporates not just specular reflection, but also diffuse reflection, absorption, and re-emission by re-radiation of the incident photons. These additional incorporated effects cause a component of the acceleration tangential to the sail, resulting in an acceleration deviating from the sail normal. This effect increases

for increasing cone angles. By comparing the control profiles of the time-optimal transfers using an ideal and optical sail model, it can be concluded that the non-ideal sail properties cause the control profile for the cone angle to be more flattened out, in other words, vary less over time. In addition, the non-ideal properties of the sail cause a 10.8% increase in transfer time to the hybrid pole-sitter at Mars. Since this result is consistent with results found in literature, a similar increase in transfer time is expected for the transfers to the other (quasi-)pole-sitters.

(b) **What is the effect of improvements in solar sail technology in a mid- to far-term time frame on the minimum-time transfer?**

To answer this question, another sensitivity analysis has been performed for the transfer to the hybrid pole-sitter at Mars. Where the baseline result has been produced using a lightness number of  $\beta = 0.05$ , in a mid- to far-term time frame a value for  $\beta$  of up to 0.1 is expected. To investigate the effect of this potential improvement in solar sail technology, time-optimal transfers for  $\beta = 0.06, 0.07, 0.08, 0.09, 0.1$  have been generated. From the results it can be concluded that the time of flight decreases when the sail performance increases, with a nearly inversely proportional relationship in this range for  $\beta$ , up to a 48.6% decrease in transfer time when the sail performance is doubled from 0.05 to 0.1.

(c) **What is the effect of the orientation of the departure orbit on the minimum-time transfer?**

One of the assumptions made in this work was that the departure orbit was a midnight-GTO, i.e., with perigee on the night-side of the Earth, exactly on the Sun-Earth line. Another sensitivity analysis has been performed, in order to check if and how this assumption affected the transfer. To this end, the other extreme has been explored: a midday-GTO, where perigee is on the day-side of the Earth. The results indeed showed a clear influence on the minimum-time transfers and the effect was different for Mars than it was for Venus. For Mars, it was observed that departing from a midday-GTO decreased the time of flight by 4.1%, while for Venus, the transfer time increased by 12.4%. From this it can be concluded that the most favorable departure GTO is one where perigee is on the day-side for transfer spiraling outwards into the Solar System and on the night-side for transfers spiraling inwards (i.e., to Venus).

2. **How does the application of a genetic algorithm compare to the use of the more conventional grid search in obtaining an initial guess for a time-optimal solar sail transfer from Earth to Mars or Venus?**

The answer to this main research question is based on the outcome of the subquestions and is therefore given after all subquestions are answered.

(a) **How does a genetic algorithm compare to the grid search in terms of feasibility and optimality of the initial guess solution?**

Both the genetic algorithm and the technique derived from dynamical systems theory (a type of grid search, hereafter referred to as DST-technique) produce near-feasible initial guesses. However, the initial guesses found using the DST-technique all have a rather large position discontinuity at the linkage of the two interplanetary phases, in the order of  $10^6$  km ( $6.7 \cdot 10^{-3}$  in non-dimensional units of the Sun-Earth circular restricted three-body problem (SE-CR3BP)). This is attributed to the fact that this technique assumes a constant clock angle,  $\delta = \pm 90^\circ$ , which means that the velocity in the out-of-plane direction cannot be controlled. Since the in- and out-of-plane motion in the CR3BP are decoupled, this results in a ballistic forward integration of the initial out-of-plane components, causing the out-of-plane component of the position to diverge farther and farther from the ecliptic. The initial state in the SE-CR3BP depends on the departure time within the year, because of the obliquity the ecliptic, which can therefore cause a significant position discontinuity, due to the explanation above. Since the genetic algorithm is able to control the out-of-plane motion, by using a clock angle different from  $\pm 90^\circ$ , it finds initial guesses with position discontinuities as small as several centimeters.

The velocity discontinuities at linkage are rather similar for both methods, between 0.27 and 0.75 km/s for the DST-technique and between 0.32 and 0.59 km/s for the genetic

algorithm. It should be noted that for both the genetic algorithm and the DST-technique initial guesses were found with a smaller velocity discontinuity, but that these transfers took much longer than the initial guesses that were selected, and were therefore considered less favorable.

Concluding, the genetic algorithm outperforms the DST-technique based on feasibility, due to the much smaller position discontinuity at linkage of the two interplanetary trajectory phases.

**(b) How does a genetic algorithm compare to the grid search in terms of ease of implementation?**

The answer to this research subquestion is twofold. On the one hand, the technique itself has to be implemented, while on the other hand, the inputs have to be tweaked in order to produce satisfying initial guesses.

First, the implementation of the techniques is compared. For both methods, the same dynamical model is used, the same bounds on the departure, arrival, and linkage dates are enforced, and the same basic principle is used: propagate forward from an initial condition, backward from a final condition, and calculate the discontinuity at linkage. These aspects are therefore not taken into account in the comparison, only the implementation of the techniques. In that case, the genetic algorithm clearly outperforms the DST-technique, because the default `ga.m` function from Matlab<sup>®</sup> could be used, while the DST-technique required much more coding.

Second, the DST-technique requires a-priori knowledge of the dynamical model and the problem at hand, to choose a suitable value for the clock angle,  $\delta$ , and a suitable range for the cone angle,  $\alpha$ . The answer to the previous subquestion 2.a already indicated that this poses a problem due to the varying initial state in the SE-CR3BP and the subsequent position discontinuity in the out-of-plane direction. In contrast, the genetic algorithm does not require any a-priori knowledge and therefore results in more feasible results based on the position discontinuity.

Concluding, the genetic algorithm outperforms the DST-technique based on ease of implementation, because of the use of a default Matlab<sup>®</sup>-function and the fact that no a-priori knowledge on the dynamical system and problem at hand is required.

**(c) How does a genetic algorithm compare to the grid search in terms of computation time?**

Before answering this subquestion, it should be noted that the computation time is of course very dependent on the coding of the techniques. However, the same holds as for subquestion 2.b: the same dynamical model is used, the same bounds on all dates, and the same basic principle. This means that any difference in computation time due to coding competency is minimized. In addition, Matlab<sup>®</sup>'s profiler has been used in order to minimize the total time spent in each function and on each line, optimizing the code as much as possible. Taking all of this into account, the genetic algorithm requires less computation time than the DST-technique, and is between 22.7% and 36.5% faster, for the four transfer cases that were investigated in this work.

Using the answers to the research subquestions above, it is possible to answer the second main research question. The genetic algorithm outperforms the DST-technique on all considered aspects: feasibility of the initial guesses, ease of implementation, and computation time. Therefore, it can be concluded that the genetic algorithm is more suitable for the generation of initial guesses for a time-optimal solar sail transfer from Earth to Mars or Venus than the grid search.

## 3.2. Recommendations

Based on the results and conclusions of this thesis, several recommendations are formulated for future work, highlighting the topics of this work that deserve attention in order to further extend the investigations on (quasi-)pole-sitters and the application of genetic algorithms in low-thrust trajectory optimization.

First, the trajectory design in this thesis can be improved by employing higher fidelity models for different elements of the design. Recall that in this work, the baseline dynamical model is the CR3BP,

complemented by an ideal solar sail and fourth-body perturbations, assuming circular ephemerides in the ecliptic plane. Many components can be replaced or added to this dynamical model, such as the implementation of the elliptic restricted three-body problem (ER3BP) to account for the eccentricity of the planets' heliocentric orbit. One step further would be to employ real ephemerides. Furthermore, currently only one fourth body is included per CR3BP, but other celestial bodies can easily be included, such as Jupiter. Also, a more accurate representation of the solar sail acceleration should be implemented, by including for example sail degradation [20].

Second, the transfers that are designed in this thesis work require an impulsive burn at perigee of the GTO of 0.76929 km/s in order to leave the Earth's sphere of influence on a parabolic escape trajectory. What would really put this mission on the map, is if it would require no high-thrust impulsive burn *at all*. This would require escape from GTO using a solar sail, which has been investigated before [21, 22]. Such a true solar sail transfer would be a substantial addition to the work already performed to investigate the feasibility of planetary (quasi-)pole-sitters.

Furthermore, as concluded in Section 3.1, the orientation of the departure orbit has an influence on the minimum-time transfer. Therefore, it is suggested that future work includes the GTO's right ascension of the ascending node as a static optimization parameter. This does not have to be implemented for the initial guess techniques, only for the optimization in PSOPT (or any other optimal control solver) and will result in even more optimal transfers.

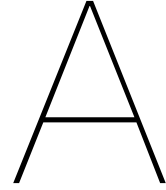
Finally, to further increase the performance of the genetic algorithm, the use of a multi-objective genetic algorithm (also implemented in Matlab<sup>®</sup>) is recommended. This multi-objective genetic algorithm will allow to not only minimize the state error at the linkage of the two interplanetary phases, but also to minimize the time of flight. Then, from the resulting Pareto front, a more calculated choice for the initial guess can be made.

### 3.3. Implications

The results obtained in the paper can be lifted to a more generic level, instead of only being interpreted based on the research questions posed in Section 1.1. This section will highlight two of these additional aspects.

While this research focused on the (quasi-)pole-sitter at Mars and Venus as the final condition of the transfer, transfers to other targets at or near these planets would result in comparable control profiles and transfer times. The recent surge in interest in Mars will undoubtedly increase the demand for cargo transport to the red planet. Since, in theory, solar sails are highly scalable, time-optimal solar sail transfers will enable the transportation of large masses to Mars. Furthermore, with the potential future habitation of Mars in mind, sail-only quasi-pole-sitters will enable permanent and continuous communication with Earth [12].

Also, since the genetic algorithm used in this work is the default `ga.m` function in Matlab<sup>®</sup>, it is implied that no sophisticated algorithm has to be coded in order to find (near-)feasible initial guesses. This means that genetic algorithms are very suitable as a first means to get an insight into the search space of a problem or at least narrow down the search space to be used by other initial guess techniques.



# Verification and Validation

This appendix elaborates on the verification and validation of the numerical techniques employed to design the transfers to (quasi-)pole-sitters at Mars and Venus to demonstrate that the obtained time-optimal transfers are correct and optimal. In order to do so, first, the dynamical model is validated, followed by the initial guess techniques, and finally the time-optimal result itself.

## A.1. Dynamical Model

The dynamical model used throughout the paper comprises several elements, namely:

1. The circular restricted three-body problem (CR3BP),
2. The ideal solar sail model,
3. The optical solar sail model,
4. Fourth-body perturbations, including simplified circular ephemerides,
5. Transformation from the Sun-planet CR3BP to the heliocentric inertial frame,
6. Transformation from the heliocentric inertial frame to the Sun-planet CR3BP.
7. Transformation from the Cartesian Earth-centered inertial frame to the SE-CR3BP.

These elements will be discussed as follows. First, the CR3BP will be validated in Section A.1.1, followed by both solar sail models in Section A.1.2 and the fourth-body perturbations in Section A.1.3. Finally, the reference frame transformations will be verified and validated in Section A.1.4.

### A.1.1. Circular Restricted Three-Body Problem

The ballistic CR3BP as discussed in Section II.A exhibits five libration points, locations of which can be found in Table A.1 [23]. When substituting the libration point locations into the dynamics, the resulting acceleration in the CR3BP should be equal to zero. Doing so results in the accelerations presented in the rightmost column of Table A.1, from which it can be concluded that the dynamics of the CR3BP are correctly implemented.

Table A.1: Locations of libration points of the SE-CR3BP [23] with the associated acceleration as calculated using the CR3BP dynamical model implemented in Matlab®.

Lagrange point	Position [non-dim]	Acceleration [non-dim]
$L_1$	[ 0.9899859823      0      0]	$4.860288 \cdot 10^{-10}$
$L_2$	[ 1.0100752000      0      0]	$1.072859 \cdot 10^{-10}$
$L_3$	[-1.0000012670      0      0]	$4.707580 \cdot 10^{-10}$
$L_4$	[ 0.4999969596      0.8660254038      0]	$3.509108 \cdot 10^{-11}$
$L_5$	[ 0.4999969596      -0.8660254038      0]	$3.509108 \cdot 10^{-11}$

### A.1.2. Solar Sail Models

To verify both solar sail models employed in this work, polar plots of the acceleration components are created, similar to Reference [24], see Fig. A.1a. The polar plot is recreated using values for the mass and lightness number equal to those used for Fig A.1a, see Fig. A.1b. The maximum acceleration associated with the ideal solar sail force bubble in Fig. A.1b is  $0.2157 \text{ mm/s}^2$ , consistent with the reference value of  $0.2155 \text{ mm/s}^2$  [24]. Furthermore, it can be seen that the force bubble for the optical sail clearly lies within the one for the ideal sail, which is also as expected. In addition to the solar sail acceleration magnitude, its direction also requires verification. Therefore, Fig. A.2a, which shows the sail pitch angle versus the cone angle [7], is reproduced in Fig. A.2b. Since updated values are used for the optical sail parameters, see Table A.2, an exact match is not expected, but qualitatively the two figures are in good agreement, thus verifying the optical sail model.

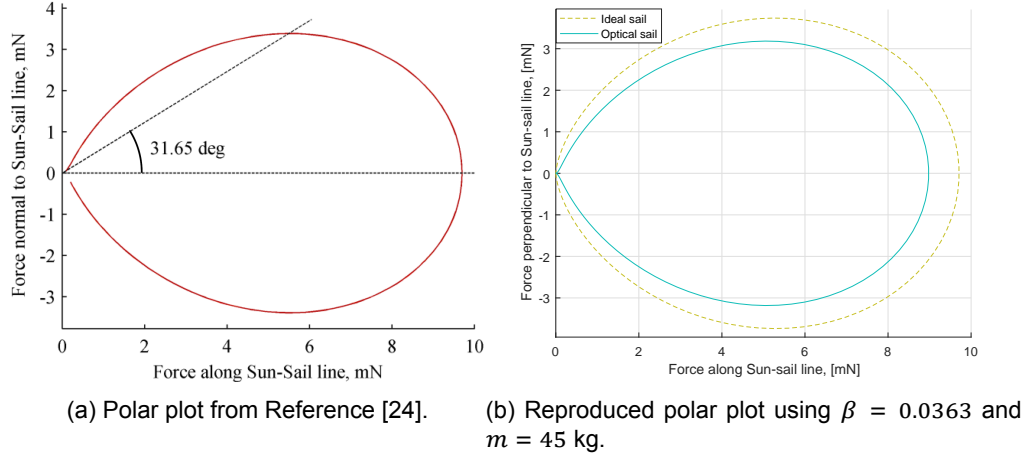


Figure A.1: Polar plots of sail performance.

Table A.2: Optical sail coefficients as used in Reference [7] and the updated values as used in this work [25].

Coefficient	Values from Halley's Comet Solar Sail mission tests, as used in Reference [7]	Updated values from Reference [25], as used in this work
$\tilde{r}$	0.88	0.91
$s$	0.94	0.94
$B_f$	0.79	0.79
$B_b$	0.55	0.67
$\epsilon_f$	0.05	0.025
$\epsilon_b$	0.55	0.27

### A.1.3. Fourth-Body Perturbation

For the sake of completeness, the equations for the fourth-body perturbation are repeated here:

$$\mathbf{a}_4 = \frac{\partial \Omega_4}{\partial \mathbf{r}_4} \quad (\text{A.1})$$

where

$$\Omega_4 = \mu_4 \left( \frac{1}{|\mathbf{r}_{s,4}|} - \frac{\mathbf{r} \cdot \mathbf{r}_4}{|\mathbf{r}_4|^3} \right) \quad (\text{A.2})$$

where  $\mathbf{r}_4$  is the position vector from the barycenter of the CR3BP to the fourth body and  $\mathbf{r}_{s,4}$  the position vector from the sail to the fourth body:  $\mathbf{r}_{s,4} = \mathbf{r}_4 - \mathbf{r}$ . Finally,  $\mu_4$  is the dimensionless gravitational parameter of the fourth body in the currently considered CR3BP.

By taking a closer look at the potential function in Eq. (A.2), two separate parts of the perturbation can be distinguished:

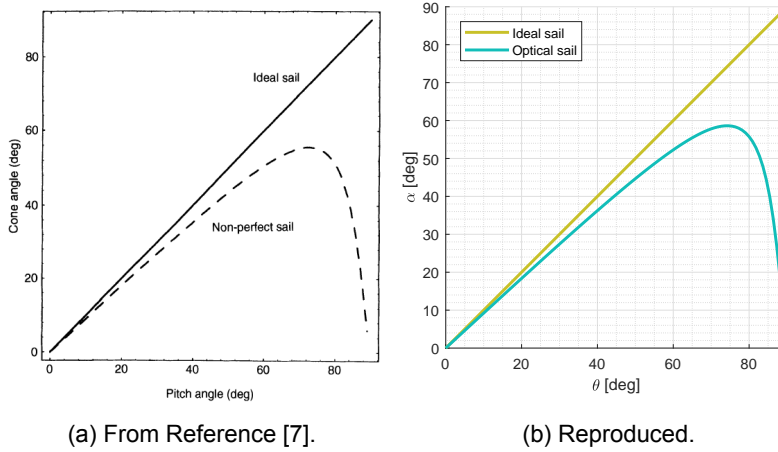


Figure A.2: Sail pitch angle vs cone angle for an optical sail.

1. The gravitational pull from the fourth body on the sail:  $\frac{\mu_4}{|\mathbf{r}_{s,4}|}$ ,
2. The change in the gravitational pull from the two primaries due to a shift of the barycenter:  $\mu_4 \frac{\mathbf{r} \cdot \mathbf{r}_4}{|\mathbf{r}_4|^3}$ .

In order to verify the fourth-body perturbations, these separate parts are calculated at various nodes along an arbitrary solar-sail trajectory in the SE-frame, with Mars as the perturbing body. This is visualized in Fig. A.3, where the nodes are connected to the position of the fourth body at that time for clarity. It can be seen in Fig. A.3, that the first part of the fourth-body perturbation acts exactly along this line, in the direction of the fourth body. The second part of the perturbation is not as trivial, but acts parallel to the line connecting the fourth body to the barycenter, as expected.

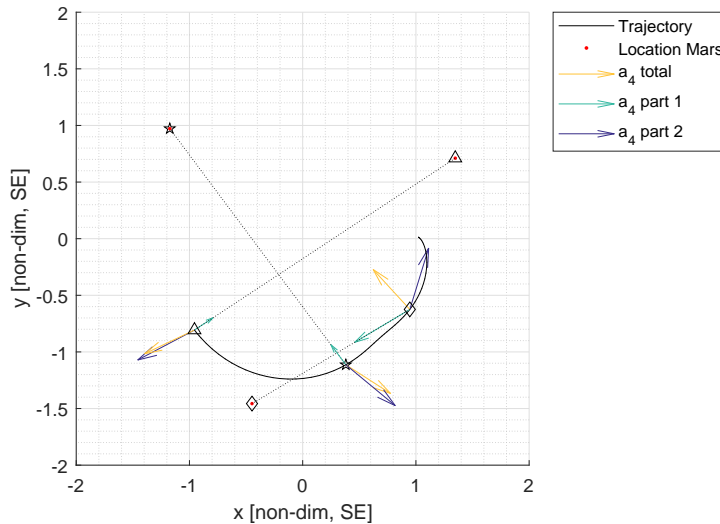


Figure A.3: Verification of fourth-body perturbation. Dotted lines connect nodes along the trajectory to the position of the fourth-body at that time. The arrows indicate the different parts of the fourth-body perturbation acceleration.

Another component of the fourth-body perturbation that has to be verified is the simplified circular ephemerides of the fourth bodies, restricted to motion in the ecliptic plane. Recall that these are calculated by using reference frame transformations, which will be verified in Section A.1.4, of the position of the planet in its own CR3BP ( $\mathbf{x} = [(1 - \mu) \ 0 \ 0 \ 0 \ 0 \ 0]$ ). The position at time  $t = 0$  can directly be verified by checking with the data obtained from NASA/JPL's Horizons online ephemeris system [26], and the remainder of the ephemeris is verified by checking whether the body moves in a coun-

terclockwise direction in the heliocentric inertial frame and completes one revolution within one year, which appeared to be the case, and thus the ephemerides are verified.

#### A.1.4. Reference Frame Transformations

In order to verify both transformations between the Sun-planet CR3BP and the heliocentric inertial frame, Fig. A.4a is reproduced. This figure shows an initial guess solution for a heteroclinic connection between halo orbits at the Sun-Earth  $L_2$ -point and the Sun-Mars  $L_1$ -point [16]. Since this initial guess solution is plotted in the SE-CR3BP, part of the trajectory requires a transformation from the SM-CR3BP to the heliocentric inertial frame and a transformation from the heliocentric inertial frame to the SE-CR3BP. Thereby, the reproduced trajectory validates both reference frame transformations at once. The small difference between the reference trajectory and the reproduced trajectory is due to the fact that the reproduced initial guess takes a little less time to get to the Mars halo orbit, as will be shown in Section A.2. Since Fig. A.4b is very similar to Fig. A.4a, these two transformations are considered verified and validated.

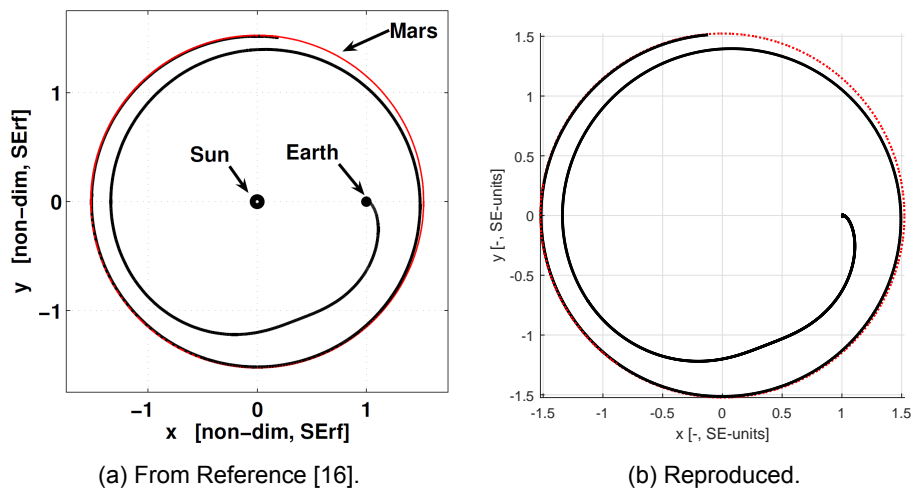


Figure A.4: Initial guess solution for a heteroclinic connection between halo orbits at the Sun-Earth  $L_2$ -point and the Sun-Mars  $L_1$ -point. Visualized in the SE-CR3BP.

The verification of the transformation from the Cartesian Earth-centered inertial reference frame to the SE-CR3BP is done by transforming the polar axis of the Earth to the SE-CR3BP, as is done in Fig. A.5a. In addition, the polar axis is transformed to the heliocentric inertial frame in Fig. A.5b, where it can be seen that the direction of the polar axis is fixed within the  $\hat{Y}\hat{Z}$ -plane (i.e., no  $\hat{X}$ -component), as expected. Thus, the transformation from the Cartesian Earth-centered inertial reference frame to the SE-CR3BP is considered verified.

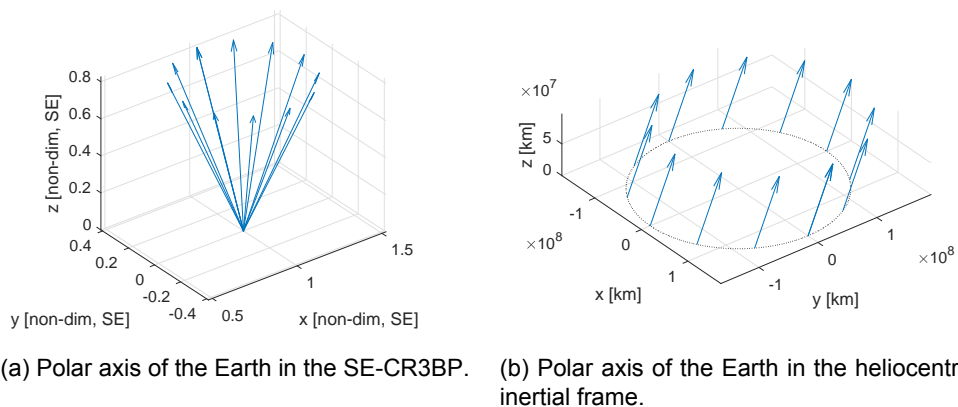


Figure A.5: Verification of the transformation from the Cartesian Earth-centered inertial reference frame to the SE-CR3BP.

## A.2. Initial Guess Techniques

Recall that the following parameters have to be obtained to find the initial guesses: departure time,  $t_{dep}$ , arrival time,  $t_{arr}$ , time at linkage of the two CR3BPs,  $t_{link}$ , and the orientation of the ideal sail (described by  $\alpha$  and  $\delta$ ) over time. The parameters found by the techniques should result in a transfer that is as feasible as possible, i.e., with small discontinuities at linkage of the two CR3BPs.

The DST-technique has been verified by reproducing the work in Reference [16], where an initial guess is obtained for a heteroclinic connection between halo orbits at the Sun-Earth  $L_2$ -point and Sun-Mars  $L_1$ -point. The technique used to produce this initial guess is slightly different from the one described in this work, because it is independent of time. However, this verification demonstrates that the method for finding the best possible initial guess using a constant sail orientation works as expected.

In Reference [16], a near-feasible initial guess is found using a constant sail orientation with  $\alpha = 62.5^\circ$  and  $\delta = 90^\circ$ . Using this information, a grid search over all combinations of 300 different points along all 200 departure and arrival trajectories is conducted and results in the most feasible possible initial guesses listed in Table A.3. These results are in good agreement with the initial guess found in Reference [16], which spans 5.83 years. The code written for the implementation of the DST-technique is thus considered verified and validated.

Table A.3: Verification of the DST-technique. Discontinuities at linkage and transfer time for a Sun-Earth  $L_2$  halo to Sun-Mars  $L_1$  halo orbit for the most feasible initial guesses using a constant sail orientation with  $\alpha = 62.5^\circ$  and  $\delta = 90^\circ$ .

#	$\Delta r$ [km]	$\Delta v$ [km/s]	Transfer time [years]
1	1974.4	0.3746	5.784
2	10096.8	0.3750	5.783
3	12146.1	0.3741	5.784
4	21099.9	0.3755	5.783
5	25406.7	0.3736	5.785

## A.3. Time-Optimal Result

Verification of the time-optimal results is a two-fold process. On the one hand, it should be demonstrated that PSOPT is capable of solving optimal control problems and locating the local minimum. On the other hand, it should be demonstrated that the solution obtained by PSOPT correctly represents the dynamical model. The latter is especially important, since the time-dependent variables (state and controls) are approximated using Legendre polynomials and not by continuous integration of the ordinary differential equations.

The first aspect, whether PSOPT is able to converge to the local minimum, is demonstrated in the PSOPT manual [27], where a range of well-known optimal control problems are solved. From this, and the fact that previous research on solar sails has been successfully performed using PSOPT [28], PSOPT is considered capable of finding optimal solutions to optimal control problems.

The second aspect, whether the solution found by PSOPT correctly represents the dynamical model, is demonstrated by propagating the initial state using the controls and time provided by PSOPT using the `ode45.m` function from Matlab<sup>®</sup>. This has been done in two ways:

1. First forward propagate the initial state at departure up to linkage, then, backward propagate the final state at arrival up to linkage and compare the states at linkage in the heliocentric inertial frame.
2. Forward propagate the initial state at departure up to arrival and compare the final state with the pole-sitter state at the arrival time in the Sun-Mars CR3BP.

Both methods interpolate the controls between the nodes provided by PSOPT using a cubic spline at 1000 intermediate points.

Results are tabulated in Table A.4, where the time-optimal transfer to the hybrid pole-sitter at Mars is reproduced using the initial state (and final state for method 1), controls and time at all nodes, all provided by PSOPT. Two observations can be made based on Table A.4. First, the way the dynamics are modeled in PSOPT with Legendre polynomials closely resembles the continuous integration of the

dynamical model as implemented in Matlab<sup>®</sup>, which is verified in Section A.1. Second, the discontinuity at linkage of the solution provided by PSOPT is very small, since propagation of this discontinuity results in a small increase in the discontinuities from method 1 to method 2.

Table A.4: Reproducing time-optimal transfer to the hybrid pole-sitter at Mars using PSOPT outputs.

	Method 1 (Discontinuity at linkage)	Method 2 (Discontinuity at pole-sitter)
$\Delta r$ [km]	3701.91	5068.29
$\Delta v$ [km/s]	$4.1719 \cdot 10^{-4}$	$9.9443 \cdot 10^{-4}$
$\Delta r$ [-, SM-units]	$1.6241 \cdot 10^{-5}$	$2.2235 \cdot 10^{-5}$
$\Delta v$ [-, SM-units]	$1.7289 \cdot 10^{-5}$	$4.1210 \cdot 10^{-5}$

# Bibliography

- [1] Ceriotti, M., and McInnes, C. R., "Systems design of a hybrid sail pole-sitter," *Advances in Space Research*, Vol. 48, No. 11, 2011, pp. 1754–1762.
- [2] McInnes, C. R., and Mulligan, P., "Final Report: Telecommunications and Earth Observations Applications for Polar Stationary Solar Sails," , 2003. Report to the National Oceanic and Atmospheric Administration from the Department of Aerospace Engineering, University of Glasgow.
- [3] Ceriotti, M., and McInnes, C. R., "Generation of optimal trajectories for Earth hybrid pole sitters," *Journal of Guidance, Control, and Dynamics*, Vol. 34, No. 3, 2011, pp. 847–859.
- [4] Ceriotti, M., and McInnes, C. R., "Hybrid solar sail and solar electric propulsion for novel Earth observation missions," *Acta Astronautica*, Vol. 69, No. 9-10, 2011, pp. 809–821. doi:10.1016/j.actaastro.2011.06.007.
- [5] Leipold, M., and Götz, M., "Hybrid Photonic/Electric Propulsion," , January 2002. Rept. SOL4-TR-KTH-0001.
- [6] Heiligers, J., van den Oever, T. D., Ceriotti, M., Mulligan, P., and McInnes, C. R., "Continuous Planetary Polar Observation from Hybrid Pole-Sitters at Venus, Earth, and Mars," *Fourth International Symposium on Solar Sailing (ISSS 2017), Kyoto, Japan, 17-20 Jan 2017*, 2016.
- [7] McInnes, C. R., *Solar sailing: technology, dynamics and mission applications.*, Springer-Praxis series in space science and technology, Berlin, 1999.
- [8] McInnes, C. R., "Solar sailing: mission applications and engineering challenges," *Philosophical Transactions of the Royal Society A: Mathematical, Physical and Engineering Sciences*, Vol. 361, No. 1813, 2003, pp. 2989–3008. doi:10.1098/rsta.2003.1280.
- [9] Russell, T. E., Heaton, A., Thomas, D., Young, R., Baysinger, M., Capizzo, P., Fabisinski, L., Hornsby, L., Maples, D., Miernik, J., and Thomas, S., *Reduction of Martian Sample Return Mission Launch Mass with Solar Sail Propulsion*, Springer Berlin Heidelberg, Berlin, Heidelberg, 2014, pp. 309–329. doi:10.1007/978-3-642-34907-2\_21.
- [10] Macdonald, M., Hughes, G., McInnes, C., Lyngvi, A., and abd Alessandro Atzei, P. F., "Solar Polar Orbiter: A Solar Sail Technology Reference Study Read More: <https://arc.aiaa.org/doi/abs/10.2514/1.16408>," *Journal of Spacecraft and Rockets*, Vol. 43, No. 5, 2006, pp. 960–972. doi:10.2514/1.16408.
- [11] McKay, R. J., Macdonald, M., Biggs, J., and McInnes, C. R., "Survey of Highly-Non-Keplerian Orbits with Low-Thrust Propulsion," *Journal of Guidance, Control and Dynamics*, Vol. 34, No. 3, 2011, pp. 645 – 666. doi:10.2514/1.52133.
- [12] Walmsley, M., Heiligers, J., Ceriotti, M., and McInnes, C. R., "Optimal Trajectories for Planetary Pole-Sitter Missions," *Journal of Guidance, Control and Dynamics*, 2016. Accepted for publication.
- [13] Heiligers, J., Ceriotti, M., McInnes, C. R., and Biggs, J. D., "Design of optimal Earth pole-sitter transfers using low-thrust propulsion," *Acta Astronautica*, Vol. 79, 2012, pp. 253–268.
- [14] Becerra, V. M., "Solving complex optimal control problem at no cost with PSOPT," *IEEE International Symposium on Computer-Aided Control System Design, Yokohama, Japan, 7-10 September, 2010*. doi:10.1109/CACSD.2010.5612676.
- [15] Vergaaij, M., and Heiligers, J., "Time-Optimal Solar Sail Heteroclinic Connections for an Earth-Mars Cycler," *68th International Astronautical Congress, Adelaide, Australia, 25-29 September, 2017*, 2017.

- [16] Mingotti, G., Heiligers, J., and McInnes, C. R., "First-guess generation of solar sail Interplanetary heteroclinic connections," *2nd IAA Conference on Dynamics and Control of Space Systems, Rome, Italy*, 2014.
- [17] Wall, B., and Conway, B. A., "Near-Optimal Low-Thrust Earth-Mars Trajectories via a Genetic Algorithm," *Journal of Guidance, Control, and Dynamics*, Vol. 28, No. 5, 2005, pp. 1027–1031. doi:10.2514/1.11891.
- [18] Dachwald, B., "Evolutionary neurocontrol: A smart method for global optimization of low-thrust trajectories," *Collection of Technical Papers - AIAA/AAS Astrodynamics Specialist Conference*, Vol. 3, 2004, pp. 1705–1720.
- [19] Rao, A., "A Survey of Numerical Methods for Optimal Control," *Advances in the Astronautical Sciences*, Vol. 135, No. 1, 2009, p. 4. doi:10.1.1.661.6337.
- [20] Dachwald, B., Mengali, G., Quarta, A., and Macdonald, M., "Parametric model and optimal control of solar sails with optical degradation," *Journal of Guidance, Control, and Dynamics*, Vol. 29, No. 5, 2006, pp. 1170–1178. doi:10.2514/1.20313.
- [21] Sacket, L. L., and Edelbaum, T. N., "Optimal solar sail spiral to escape," *Astrodynamics Specialist Conference; Sept. 7-9, 1977; Jackson Hole, WY; US, 1977*.
- [22] Coverstone-Carroll, V. L., and Prussing, J. E., "Technique for Escape from Geosynchronous Transfer Orbit Using a Solar Sail," *Journal of Guidance, Control, and Dynamics*, Vol. 26, No. 4, 2003.
- [23] Parker, J., *Low-energy Ballistic Lunar Transfers*, University of Colorado at Boulder, 2007.
- [24] Heiligers, J., Diedrich, B., Derbes, B., and McInnes, C. R., "Sunjammer: Preliminary end-to-end mission design." *AIAA/AAS Astrodynamics Specialist Conference 2014*, 2014.
- [25] Heaton, A., Ahmad, N., and Miller, K., "Near Earth Asteroid Scout Solar Sail Thrust and Torque Model," *4th International Symposium on Solar Sailing (ISSS 2017), 17-20 Jan. 2017, Kyoto, Japan, 2017*.
- [26] NASA, Jet Propulsion Laboratory, "HORIZONS Web-Interface," <https://ssd.jpl.nasa.gov/horizons.cgi>, Accessed on: June 21, 2017, 2017.
- [27] Becerra, V., *PSOPT Optimal Control Solver User Manual*, 2011.
- [28] Heiligers, J., Mingotti, G., and McInnes, C. R., "Optimisation of solar sail interplanetary heteroclinic connections," *2nd Conference on Dynamics and Control of Space Systems, Rome, Italy*, 2014.



